Article

# Chemoproteomic discovery of a covalent allosteric inhibitor of WRN helicase

https://doi.org/10.1038/s41586-024-07318-y

Received: 19 October 2023

Accepted: 14 March 2024

Published online: 24 April 2024

Check for updates

Kristen A. Baltgalvis[1], Kelsey N. Lamb[1], Kent T. Symons[1], Chu-Chiao Wu[1], Melissa A. Hoffman[1], Aaron N. Snead[1], Xiaodan Song[1], Thomas Glaza[1], Shota Kikuchi[1], Jason C. Green[1], Donald C. Rogness[1], Betty Lam[1], Maria E. Rodriguez-Aguirre[1], David R. Woody[1], Christie L. Eissler[1], Socorro Rodiles[1], Seth M. Negron[1], Steffen M. Bernard[1], Eileen Tran[1], Jonathan Pollock[1], Ali Tabatabaei[1], Victor Contreras[1], Heather N. Williams[1], Martha K. Pastuszka[1], John J. Sigler[1], Piergiorgio Pettazzoni[2], Markus G. Rudolph[2], Moritz Classen[2], Doris Brugger[2], Christopher Claiborne[2], Jean-Marc Plancher[2], Isabel Cuartas[3], Joan Seoane[3], Laurence E. Burgess[1], Robert T. Abraham[1,4], David S. Weinstein[1], Gabriel M. Simon[1], Matthew P. Patricelli[1]✉ & Todd M. Kinsella[1]✉

WRN helicase is a promising target for treatment of cancers with microsatellite instability (MSI) due to its essential role in resolving deleterious non-canonical DNA structures that accumulate in cells with faulty mismatch repair mechanisms[1–5]. Currently there are no approved drugs directly targeting human DNA or RNA helicases, in part owing to the challenging nature of developing potent and selective compounds to this class of proteins. Here we describe the chemoproteomics-enabled discovery of a clinical-stage, covalent allosteric inhibitor of WRN, VVD-133214. This compound selectively engages a cysteine (C727) located in a region of the helicase domain subject to interdomain movement during DNA unwinding. VVD-133214 binds WRN protein cooperatively with nucleotide and stabilizes compact conformations lacking the dynamic flexibility necessary for proper helicase function, resulting in widespread double-stranded DNA breaks, nuclear swelling and cell death in MSI-high (MSI-H), but not in microsatellite-stable, cells. The compound was well tolerated in mice and led to robust tumour regression in multiple MSI-H colorectal cancer cell lines and patient-derived xenograft models. Our work shows an allosteric approach for inhibition of WRN function that circumvents competition from an endogenous ATP cofactor in cancer cells, and designates VVD-133214 as a promising drug candidate for patients with MSI-H cancers.

Cancers with microsatellite instability (MSI) result from mutations in mismatch repair genes, including *MLH1*, *MSH2*, *MSH6* and *PMS2* (ref. 6), leading to broadly distributed insertions and/or deletions of TA-dinucleotide repeats within microsatellite regions across the genome. Expanded TA repeats can form problematic DNA secondary structures during replication that must be resolved before cells enter mitosis, to avoid potentially lethal consequences. The frequency of MSI across all cancer types is 4%, with higher frequencies in endometrial carcinoma (30%), colon adenocarcinoma (20%) and gastric adenocarcinoma (20%)[7,8]. The current standard of care for MSI-high (MSI-H) cancers includes surgery, chemotherapy and immunotherapy[9,10]. Immunotherapy has been successful in treating patients with MSI-H cancers but intrinsic or acquired resistance can diminish clinical responses[11–14], creating a need for alternative therapies for this disease.

WRN is one of five members of the RecQ family of DNA helicases and was recently identified as a synthetic lethal vulnerability in MSI-H cancers by four independent groups[1–4]. WRN is a nuclear protein with two known enzymatic functions: a 3′–5′ exonuclease activity residing in the amino-terminal region[15] and ATP-dependent 3′–5′ DNA helicase unwinding activity[16]. The helicase activity, but not the exonuclease, of WRN plays an essential and non-redundant role in the resolution of DNA secondary structures formed by expanded TA-dinucleotide repeats in MSI-H cancers[1–4]. Loss of WRN function leads to double-stranded DNA (dsDNA) breaks, chromosome shattering and cell death, specifically in MSI-H tumour cells but not in healthy cells[1–5,17], because only MSI-H cells contain widespread expansions of vulnerable microsatellite regions. The robust synthetic lethal relationship between WRN and MSI cancer makes this a highly attractive target in multiple cancers with MSI.

## Discovery of covalent WRN ligands

We developed a targeted mass spectrometry-based chemoproteomics method to quantify the covalent binding of small molecules to cysteine residues in native cells or cell lysates (Fig. 1a). This platform measures

[1]Vividion Therapeutics, San Diego, CA, USA. [2]Pharma Research and Early Development pRED F. Hoffmann-La Roche, Ltd, Basel, Switzerland. [3]Vall d'Hebron Institute of Oncology, Vall d'Hebron University Hospital, Universitat Autònoma de Barcelona, CIBERONC, Barcelona, Spain. [4]Present address: Odyssey Therapeutics, San Diego, CA, USA. ✉e-mail: mattp@vividion.com; tkinsella71c@gmail.com

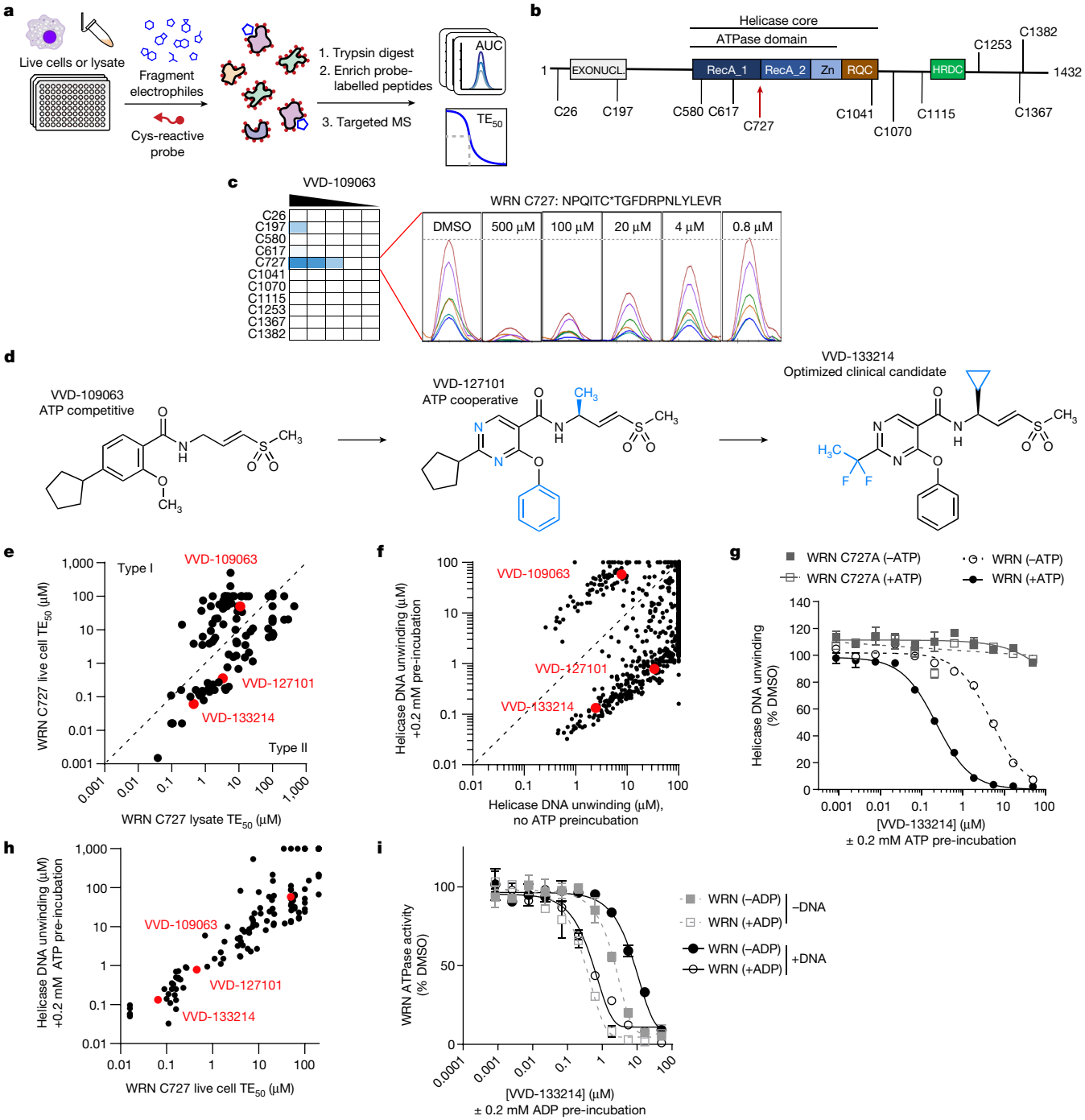


**Fig. 1 | Discovery of a covalent WRN inhibitor, VVD-133214, using chemoproteomics. a**, General protocol for chemoproteomics-based inhibitor discovery: live cells or cell lysates are treated with DMSO or inhibitors in a 96-well plate. Inhibitor binding prevents cysteine residues from reacting with the probe, and probe-enriched peptides are measured using label-free parallel reaction monitoring mass spectrometry (MS). Target engagement (TE) is calculated by comparison of areas under the curve (AUCs) of inhibitor-treated and control wells and can be curve-fitted to determine $TE_{50}$ values. **b**, Location of probe-accessible cysteines (C) on WRN subjected to chemoproteomics screening. **c**, Discovery of VVD-109063 as a WRN C727 binder with an approximate $TE_{50}$ of 10 µM in lysates and good selectivity for C727. **d**, Progression of WRN C727 series from the initial VVD-109063 hit to the more advanced ATP-cooperative compounds VVD-127101 and VVD-133214. **e**, Comparison of $TE_{50}$ in lysates versus live cells demonstrates distinct populations of compounds showing either reduced or enhanced potency in live cells relative to lysates. **f**, Comparison of WRN helicase ($hWRN^{519–1227}$) DNA unwinding activity with or without 0.2 mM ATP during the compound preincubation period demonstrated two distinct populations showing either competitive activity (for example, VVD-109063) or cooperative inhibitory activity (for example, VVD-127101 and VVD-133214). **g**, Inhibition of $hWRN^{519–1227}$ (wild type (WT) and C727A) by VVD-133214 with or without ATP during the compound preincubation period. **h**, Correlation between live cell WRN C727 engagement and biochemical $hWRN^{519–1227}$ helicase activity plus 0.2 mM ATP during the compound preincubation period. **i**, ATPase activity of $hWRN^{519–1227}$ in the presence of VVD-133214 with or without ADP preincubation and DNA substrate. $IC_{50}$ derived from $n = 2$ biologically independent samples and presented as means ± s.e.m.

changes in the accessibility of cysteine residues using a biotinylated iodoacetamide-based covalent probe (IAA probe) and provides a sensitive way to detect the binding of covalent small molecules to cysteine residues[18,19]. Although the throughput of this method is modest relative to focused biochemical screening, it permits simultaneous evaluation of both the potency and selectivity of molecules against hundreds of proteins in their native state. We used this method to screen a custom library of several thousand electrophilic small molecules in native cell lysates against cysteine residues on over 300 proteins with critical roles in cancer and/or immune diseases, including 11 solvent-exposed cysteine residues on WRN (Fig. 1b). A series of compounds, represented by VVD-109063, was identified that selectively engaged C727 on WRN with half-maximal target engagement ($TE_{50}$) potency in the low-micromolar range following 1 h of treatment (Fig. 1c–e). C727 is located on the opposite face of the protein relative to the ATP-binding site and had not been identified as having functional relevance at the time of screening. A helicase assay was performed using purified human WRN core helicase domain (fragments 519–1,227; $hWRN^{519–1227}$), and VVD-109063 was found to be an inhibitor with a half-maximal inhibitory concentration ($IC_{50}$) of 8 µM (Fig. 1f). While this manuscript was in preparation, Parker et al. reported that covalent engagement of WRN C727 with a small molecule (H3B-968) had the potential to inhibit WRN function in vitro using purified WRN protein, but not in cells[20]. To further characterize our compounds we measured the C727 engagement potency of VVD-109063 and related compounds in live OCI-AML2 cells. Interestingly, two classes of compound emerged from this in cellulo analysis: one subset that showed reduced potency in live cells relative to cell lysates (Type I, exemplified by VVD-109063; Fig. 1e) and another that showed improved potency in live cells relative to lysates (Type II, exemplified by VVD-127101; Fig. 1e). An off-target cysteine shared by many of these early-hit compounds, C54 from TNFAIP3, showed equipotent engagement in lysates and live cells across both types of molecule (Extended Data Fig. 1a), suggesting that differences in cell permeability were probably not contributing significantly to the potency discrepancy in cells. We considered that ATP levels, which are high in live cells but low in cell lysates (due to substantial sample dilution during preparation), were another possible explanation for these distinct behaviours. For direct assessment of this possibility, the helicase assay was adapted to include ATP during the compound preincubation step with $hWRN^{519–1227}$, and the results confirmed that Type I compounds lost potency when ATP was included during the compound preincubation step whereas Type II compounds showed significant improvement in potency in the presence of ATP (Fig. 1f,g and Extended Data Fig. 1b). We found a strong overall correlation between $TE_{50}$ values in live cells and $IC_{50}$ values for helicase inhibition in the presence of ATP for both Type I and II compounds (Fig. 1h). On the basis of favourable live cell potency, apparent nucleotide-cooperative behaviour and a favourable global cysteine selectivity profile for the Type II series (Extended Data Fig. 1c), we chose to optimize this series further. Subsequent lead optimization afforded the clinical candidate, VVD-133214 (Fig. 1d; details of the medicinal chemistry campaign will be described elsewhere). VVD-133214 showed potent cellular $TE_{50}$ values (Fig. 1e,h and Extended Data Fig. 1d) and was equally active in both human and mouse WRN helicase ($mWRN^{486–1232}$) DNA unwinding assays (Extended Data Fig. 1e). We also confirmed inhibition of $hWRN^{519–1227}$ ATPase activity in the absence of DNA (Fig. 1i), selectivity for $hWRN^{519–1227}$ over the closely related human BLM helicase ($hBLM^{636–1298}$; Extended Data Fig. 1f) and the requirement for covalency using either C727A-mutated hWRN (Fig. 1g) or a non-electrophilic analogue (VVD-129448) (Extended Data Fig. 1g). Consistent with the lack of inhibition exerted by the non-electrophilic analogue, there was no evidence of saturation of covalent engagement kinetics ($k_{obs}$) up to 15 µM (Extended Data Fig. 1h and Extended Data Table 1), which was the highest concentration that could be tested without stop-flow equipment.

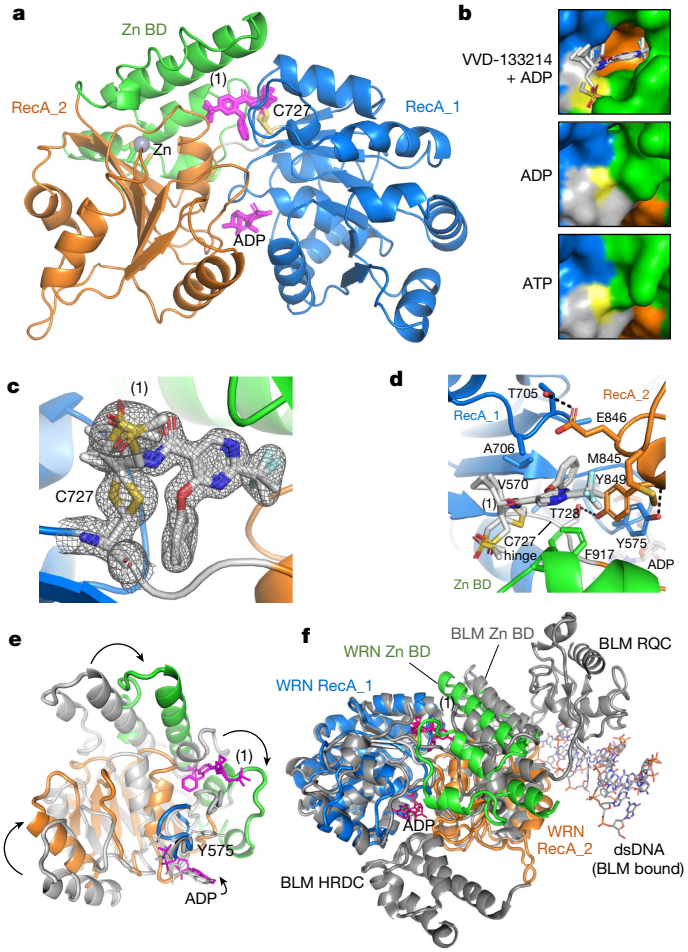


**Fig. 2 | Overall architecture of the closed conformation of the WRN helicase domain. a**, N-terminal RecA_1 domain (blue) connected by a hinge (grey) to the C-terminal RecA_2 domain (orange) and zinc-binding domain (Zn BD, green). The zinc ion and its four cysteine residues are shown. ADP is bound at the bottom and the covalent inhibitor VVD-133214 (1, pink) is bound at the top of the ATPase domain. **b**, Surface view of the ligand-binding pocket in the VVD-133214 + ADP, ADP and ATP structures (Protein Data Bank (PDB) 7GQU, 7GQS and 7GQT, respectively). **c**, 2Fo–Fc electron density map at 1.5 $\sigma$ for VVD-133214 highlighting nucleophilic attack on the C727 Sγ atom in two different orientations. **d**, WRN side chains engaging in van der Waals interactions with VVD-133214 are labelled. No direct hydrogen bonds exist between the inhibitor and WRN. Interdomain hydrogen bonds are shown as dashed lines, indicating closure of the helicase core. **e**, Comparison of WRN ADP-bound (grey) and VVD-133214 + ADP-bound (coloured) structures showing conformational changes to the WRN RecA_2, Zn-binding domain, Tyr575 in the Walker A motif, and ADP between the structures. **f**, Superposition of WRN in complex with VVD-133214 (1) and the closely related BLM helicase in complex with a dsDNA carrying a single-stranded DNA overhang (PDB 4CGZ)[35].

## Characterization of structure and mechanism

We determined the crystal structure of the WRN ATPase domain, encompassing residues 517–945, in complex with either adenosine diphosphate (ADP), ATP or VVD-133214 plus ADP. The WRN-VVD-133214 cocrystal structure was solved at 1.54 Å resolution (Extended Data Table 2) and showed that VVD-133214 binds within a hydrophobic pocket at the interface between the RecA_1 and RecA_2 domains of the ATPase (Fig. 2a,b). Clear electron density was observed connecting the sulfur atom of C727 and beta-carbon of the vinyl sulfone of VVD-133214 (Fig. 2c). The absence of hydrogen bonding interactions between VVD-133214 and WRN suggests that shape complementarity and relatively weak reversible interactions are sufficient to properly

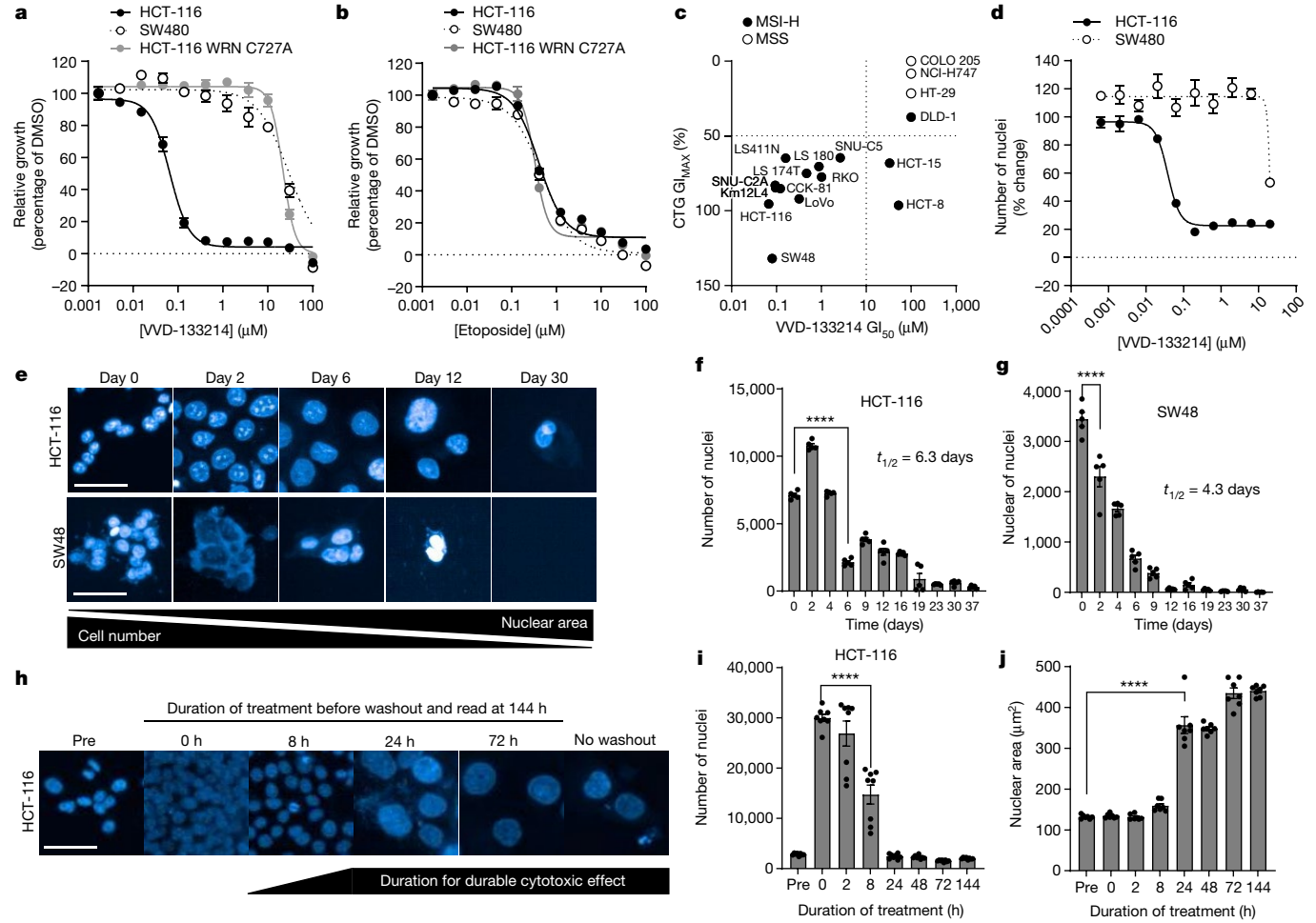


**Fig. 3 | VVD-133214 inhibits growth in MSI-H cells but not in MSS.** **a**, VVD-133214 potently inhibits cell growth in MSI-H HCT-116 cells (black circles; $GI_{50}$ = 0.066 ± 0.007 μM, $n$ = 2 biologically independent samples) but in neither MSS SW480 (white circles; $GI_{50}$ > 20 μM, $n$ = 2) nor HCT-116 WRN C727A mutant cells (grey circles; $GI_{50}$ > 20 μM, $n$ = 2) following 5 days of compound treatment using a CellTiter-Glo (CTG) assay. **b**, The potency of etoposide was similar in MSI-H HCT-116 cells ($GI_{50}$ = 0.406 ± 0.057 μM, $n$ = 2) and MSS SW480 cells ($GI_{50}$ = 0.479 ± 0.081 μM, $n$ = 2). **c**, A panel of 14 MSI-H (filled circles) and three MSS (empty circles) colorectal cancer cell lines were screened in a 5 day CTG assay for comparison of $GI_{50}$ and maximal growth inhibition ($GI_{MAX}$). Cell lines were designated as sensitive (lower left quadrant) if $GI_{50}$ < 10 μM and $GI_{MAX}$ > 50%. **d**, Hoechst-based imaging used to quantitate nuclear number in a 5 day assay comparing VVD-133214 activity in MSI-H (HCT-116, filled circles; $GI_{50}$ = 0.038 ± 0.006 μM, $n$ = 4) and MSS cells (SW480, empty circles; $GI_{50}$ > 20 μM, $n$ = 4). **e**–**g**, Hoechst-based imaging (**e**) was used to quantitate nuclear number following VVD-133214 treatment (2 μM) for up to 30 days in MSI-H HCT-116 (**f**) and SW48 cells (**g**); scale bars, 50 μm. **h**–**j**, Short-term treatment of HCT-116 cells with 2 μM VVD-133214 followed by washout of the compound (**h**) for a 6 day assay assessing nuclear number (**i**) and area (**j**) ($n$ = 7–8 biologically independent samples); scale bar, 50 μm. Data shown as means ± s.e.m. $GI_{50}$ data reported are ±s.d. and were analysed by one-way analysis of variance (ANOVA), ****$P$ < 0.0001 versus $t_0$.

align the vinyl sulfone electrophile for nucleophilic attack by C727. Analogous cases have also been observed for other covalent inhibitors and point to important differences in the types of molecular features that ultimately determine potency and selectivity of covalent versus reversible binders[21]. As demonstrated here, these differences can be exploited to probe new target space and develop drugs to proteins previously regarded as 'undruggable'.

The VVD-133214-binding pocket sits within a flexible hinge region subject to interdomain movement located 12.3 Å away from the nucleotide-binding site (Fig. 2a). The binding of VVD-133214 results in major structural rearrangements relative to unliganded WRN that lead to a closed conformation stabilized by a series of hydrogen bonds forming between the RecA_2 domain (T705), RecA_1 domain (E846 and Y849), Walker A motif (Y575) and the hinge region (T728; Fig. 2d,e). Importantly, Y575 flips to form an H-bond with the backbone carbonyl of Y849, whose side chain makes direct contact with VVD-1333214. This molecular network establishes a potential explanation for the nucleotide-cooperative binding of VVD-133214 because the bound nucleotide shifts in the liganded state. Stabilization of WRN in a closed state has implications for its ability to participate in multiturnover helicase reactions[22], and is a plausible explanation for WRN inhibition by VVD-133214. VVD-133214 showed no effect on DNA binding (Extended Data Fig. 1i), suggesting that the primary mechanism of action involves inhibition of ATPase activity. Furthermore we observed that, when WRN is actively unwinding DNA, time-dependent inhibition is lost (Extended Data Fig. 1j), implying that VVD-133214 targets the pre-DNA-bound state of WRN. Importantly, we found that the crystallization construct used here, which lacks the HRDC domain, shows significantly reduced engagement potency in the presence of ADP compared with constructs containing this domain (Extended Data Fig. 1k), suggesting that the HRDC domain may contribute to some aspect of compound binding (Fig. 2f).

## VVD-133214 is cytotoxic in MSI-H cells

VVD-133214 was tested in a 5 day cell proliferation assay, in which we found that the compound decreased the growth of MSI-H HCT-116 cells

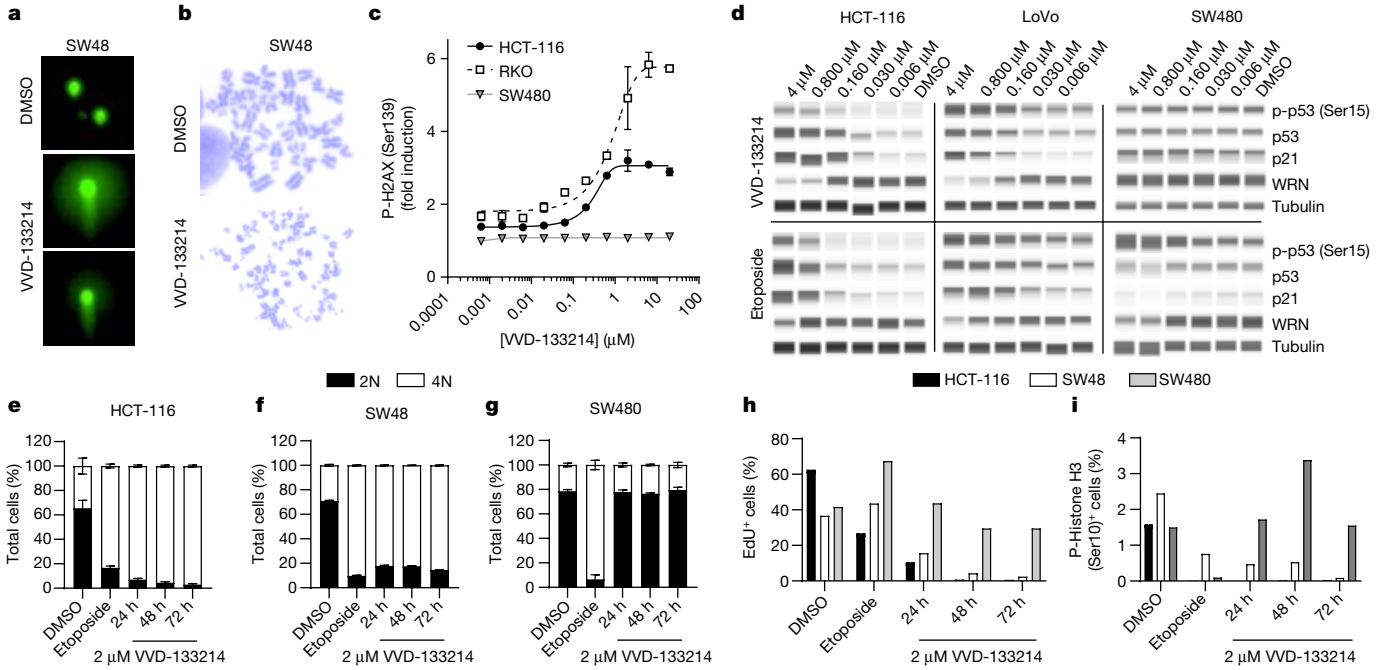


**Fig. 4 | VVD-133214 induces DNA damage-and-repair response in MSI-H cells. a**,**b**, Representative images of DNA damage by Comet assay (**a**) and metaphase spread (**b**) in MSI-H SW48 cells. **c**, Quantitation of P-H2AX induction by immunofluorescence following VVD-133214 treatment in cell lines HCT-116, RKO and SW480; $n = 2$ biologically independent experiments. **d**, Representative immunoblots of p-p53 (Ser15), total p53, p21 and WRN in MSI-H HCT-116, MSI-H LoVo and MSS SW480 cells. **e**–**g**, Cell cycle assessment following treatment with 2 μM VVD-133214 or 2 μM etoposide for DNA content in HCT-116 (**e**), SW48 (**f**) and SW480 cells (**g**); $n = 2$ biologically independent samples. **h**, Percentage of cells in S-phase demonstrated by EdU labelling. **i**, Percentage of cells in mitosis demonstrated by phospho-histone (P-Histone) H3 (Ser10) staining. Data shown as means s.e.m. Micrographs are representative of two independent experiments with similar results.

but not microsatellite-stable (MSS) SW480 (Fig. 3a). By contrast, the topoisomerase II inhibitor etoposide impaired cell growth to an equivalent degree in HCT-116 and SW480 cells (Fig. 3b). The antiproliferative effect of VVD-133214 in HCT-116 cells was blocked by the introduction of a drug-resistant C727A WRN mutant (Fig. 3a), confirming on-target antiproliferative activity. An expanded analysis showed that nearly 80% of MSI-H cell lines (11 of 14) tested were sensitive to VVD-133214 whereas none of the MSS cell lines (HT-29, COLO 205 and NCI-H747) appeared responsive (Fig. 3c). The three MSI-H cell lines that were insensitive to VVD-133214 (DLD-1, HCT-15 and HCT-8) also have not shown genetic dependency on WRN in DepMap[23] or other studies[1,3,4]. These data, taken together, demonstrate that VVD-133214 is capable of driving synthetic lethality in MSI-H colorectal cancer cells through covalent inhibition of WRN.

High-content imaging showed that MSI-H HCT-116 cells treated with VVD-133214 continued to proliferate for 2–3 days, followed by a steady decline with very few cells remaining at the end of the 37 day assay period (Fig. 3d–f). The impact on MSI-H SW48 cells was more rapid, with decreases in cell numbers already apparent by day 2 and near-complete cell loss by day 12 (Fig. 3e,g). Washout experiments demonstrated that exposure times of only 2–8 h were partially efficacious whereas 24 h of exposure to VVD-133214 produced a sustained cytotoxic effect in both MSI-H lines tested (Fig. 3h,i and Extended Data Fig. 2a,b).

Imaging also showed that treatment with VVD-133214 increased the nuclear area of HCT-116 cells by three- to fourfold when measured after 6 days, and this morphological change required only 24 h treatment followed by compound washout (Fig. 3e,h,j). A similar, albeit less robust, response was seen in LoVo cells (Extended Data Fig. 2a,c). Increases in nuclear area have also been reported following genetic perturbation of WRN or in cells expressing helicase-dead WRN mutants[3,4,24]. These changes in nuclear size are more consistent with a senescent phenotype[25] than an apoptotic effect (Extended Data Fig. 3a–d) and were also observed with etoposide[26] and radiation treatment[27], suggesting commonalities in the downstream molecular mechanisms leading to cell death, such as induction of dsDNA breaks and widespread loss of chromosomal integrity.

## DNA damage and G2 arrest in MSI-H cells

WRN is required for unwinding problematic DNA structures found in MSI-H cells, and the loss of WRN during cell replication leads to dsDNA breaks and the initiation of a DNA repair response[1–5]. Treatment of MSI-H SW48 cells with VVD-133214 for 24–48 h led to the appearance of comet tails and loss of intact chromosomes, both of which are indicative of DNA damage (Fig. 4a,b). In addition, 96 h VVD-133214 treatment of MSI-H RKO and HCT-116 cells, but not of MSS SW480 cells, caused a three- to fivefold induction of phospho-H2AX, consistent with the induction of dsDNA breaks[28] following loss of WRN expression[2,3] (Fig. 4c and Extended Data Fig. 4a). Similarly, concentration-dependent induction of other DNA damage responses, such as phospho-p53 (p-p53), total p53 and p21, were noted in VVD-133214-treated MSI-H HCT-116 and LoVo cells, but not in MSS SW480 cells (Fig. 4d and Extended Data Figs. 3e–g and 4b–d). The selective induction of DNA damage in MSI-H cell lines by VVD-133214 was also associated with strong G2 arrest, as evidenced by an increase in 4 N DNA content and a reduction in cells entering S-phase and mitosis (Fig. 4e–i and Extended Data Fig. 3h–k).

Interestingly, WRN protein levels were also reduced by VVD-133214 in a concentration-dependent manner by as much as 89% in MSI-H cells but not in MSS cells (Fig. 4d and Extended Data Figs. 3m–o and 4e,f). Loss of WRN in the presence of VVD-133214 was inhibited by the proteasome inhibitor bortezomib and was not impacted by cycloheximide, suggesting direct loss of protein rather than altered transcription or

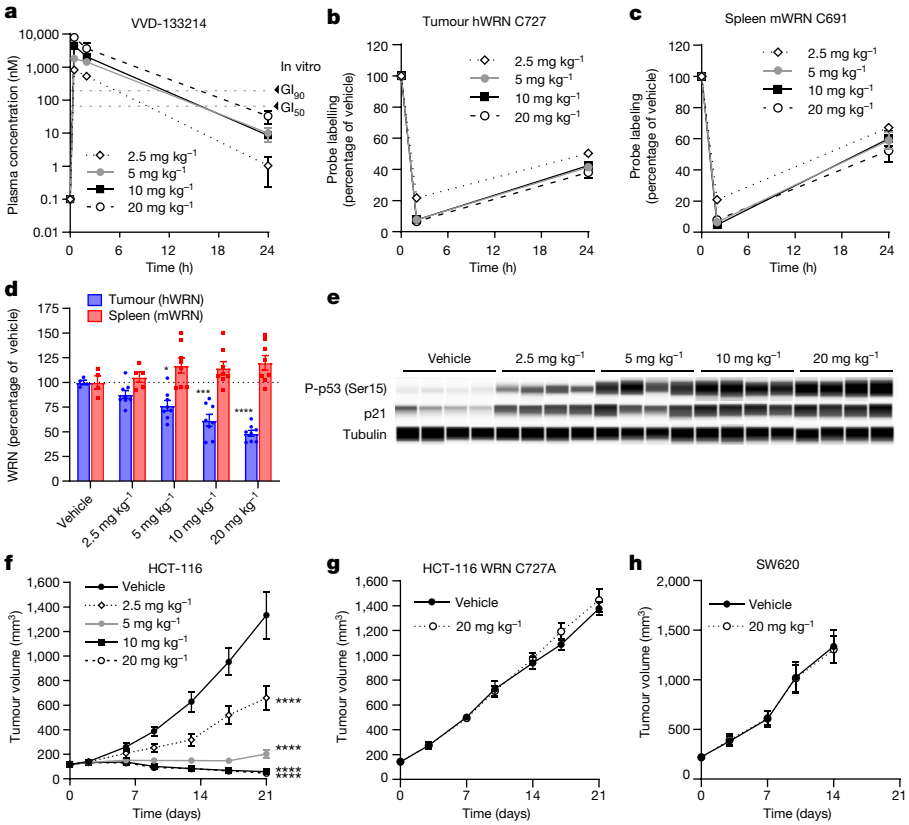


**Fig. 5 | Pharmacokinetics/pharmacodynamics and tumour growth inhibition in MSI-H colorectal cancer xenograft models. a–h**, VVD-133214 was dosed daily at 2.5, 5, 10 or 20 mg kg$^{-1}$ via oral administration for 4 days. Tissues were collected at 2 and 24 h following the last dose ($n = 4$ per group). **a**, Plasma exposures of VVD-133214 at 2 or 24 h after the last dose. Grey horizonal dashed lines indicate plasma concentrations equivalent to in vitro $GI_{50}$ and $GI_{90}$ of VVD-133214-treated HCT-116 cells (uncorrected for plasma protein binding). **b**,**c**, WRN C727 engagement in HCT-116 xenograft tumour (**b**) and C691 engagement in mouse spleen (**c**), as measured by mass spectrometry. Average probe labelling in vehicle-treated animals was defined as 100%. **d**, Total WRN protein in tumour and spleen as measured by mass spectrometry. **e**, Simple immunoblot analysis for p-p53 (Ser15) and p21 in tumours 24 h following the last dose. **f–h**, Growth was measured for WT HCT-116 (**f**), HCT-116 WRN C727A (**g**) and SW620 (MSS) tumours (**h**) in female homozygous Foxn1 <nu> mice dosed orally with 2.5, 5, 10 or 20 mg kg$^{-1}$ VVD-133214 every day for 3 weeks ($n = 8$ per group). Data shown as means ± s.e.m. and were analysed by one-way ANOVA, $^{*}P < 0.05$, $^{**}P < 0.01$, $^{***}P < 0.001$, $^{****}P < 0.0001$.

translation (Extended Data Figs. 4g and 3l). We considered that loss of WRN could have resulted from VVD-133214-induced cell cycle arrest, but no cell cycle-related changes in WRN expression were observed in nocodazole-synchronized HCT-116 cells (Extended Data Fig. 4h). We did find that at least some of the loss of WRN in VVD-133214-treated cells could be attributed to a general DNA damage response mechanism, because the DNA damage-inducing agent etoposide likewise decreased WRN content in both MSI-H and MSS cells (Fig. 4d and Extended Data Figs. 3m–o and 4f).

## VVD-133214 inhibits WRN in vivo

Given the robust in vitro activity observed in MSI-H cell lines, we progressed to in vivo studies in tumour-bearing mice. Once-daily oral treatment with VVD-133214 at 5 mg kg$^{-1}$ or higher resulted in near-complete target engagement within the tumour (approximately 95%) and plasma exposures that were maintained above in vitro 50% growth inhibition ($GI_{50}$) (0.066 µM in HCT-116 cells) for at least 8 h (Fig. 5a,b). By 24 h post dosing, clearance-mediated reductions in compound exposure, combined with WRN protein resynthesis (13 h in vitro protein half-life), reduced WRN engagement levels to 60–70% at all doses (Fig. 5b). Similar to observations made in vitro, protein abundance of WRN within tumours was consistently decreased in treated mice (Fig. 5d) and this appeared to be dependent on MSI-H status because there was no change in mouse WRN protein abundance in the spleen, despite high levels of WRN engagement in this tissue (equivalent cysteine in mouse WRN is C691) (Fig. 5c,d)

Tumours were also assessed for markers of DNA damage following the last dose of VVD-113214. P-p53 levels increased by between seven- and 12-fold and P21 protein levels increased by two- to threefold across VVD-133214 doses of 5, 10 and 20 mg kg$^{-1}$ relative to vehicle treatment (Fig. 5e and Extended Data Fig. 5a–c), with no significant difference between the 10 and 20 mg kg$^{-1}$ dose groups. These data suggest that daily dosing with 10–20 mg kg$^{-1}$ VVD-133214 is sufficient to induce near-maximal WRN C727 engagement and DNA damage responses in mice bearing MSI-H xenografts.

## VVD-133214 causes MSI-H tumour regression

In mice, once-daily oral administration of VVD-133214 for 3 weeks resulted in dose-dependent inhibition of MSI-H HCT-116 tumour xenograft growth (Fig. 5f) without impacting body mass (Extended Data Fig. 5d). The two lower doses resulted in varying levels of tumour growth inhibition (up to 93%) whereas the 10 or 20 mg kg$^{-1}$ day$^{-1}$ doses demonstrated 51 and 61% tumour regression, respectively (Fig. 5f), consistent with near-maximal levels of target engagement, DNA damage marker induction and WRN protein loss (50–60%) achieved with the 10 mg kg$^{-1}$ day$^{-1}$ dose (Fig. 5e and Extended Data Fig. 5c).

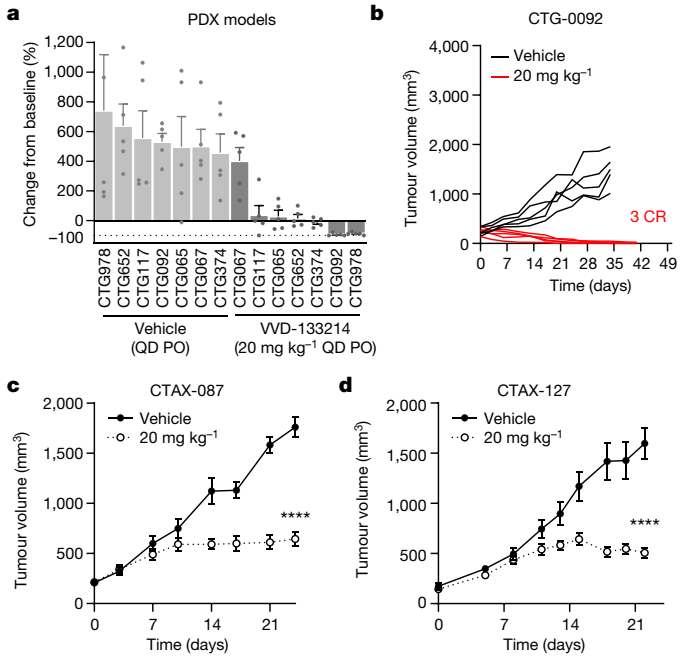


**Fig. 6 | VVD-133214 inhibits tumour growth in MSI-H PDX models.** **a**–**d**, Mice bearing MSI-H colorectal cancer PDXs were dosed orally with either VVD-133214 or vehicle daily ($n = 5$ per group). **a**, Average percentage change from baseline in tumour volume at study end. **b**–**d**, Spider plots of CTG-0092 PDX model (**b**) and immunotherapy-refractory PDX models CTAX-087 (**c**) and CTAX-127 (**d**). Mice were dosed orally with either VVD-133214 or vehicle daily ($n = 10$ per group). CR, complete response. Data are shown as means ± s.e.m. and were analysed by two-way ANOVA with Tukey's multiple-comparison test, $^{****}P < 0.0001$.

Similar tumour growth-inhibitory effects were observed for VVD-133214 in additional MSI-H xenograft models LoVo and SW48 (Extended Data Fig. 5e,f). By contrast, VVD-133214 did not affect tumour growth rates of HCT-116 xenografts expressing a C727A WRN mutant (Fig. 5g), or of MSS xenografts SW620 (Fig. 5h) and SW480 (Extended Data Fig. 5g). The absence of any tumour growth-inhibitory effect in MSS xenografts correlates with unchanged markers of DNA damage (Extended Data Fig. 5h). These data provide compelling evidence that covalent inhibition of WRN leads to robust tumour growth inhibition in preclinical models of MSI-H cancer.

Patient-derived xenograft (PDX) models have gained traction in the evaluation of preclinical drugs due to the retention of genetic signatures from patients, heterogeneity within tumours and the development of resistance to therapies in the clinic[29]. Accordingly, we tested VVD-133214 in a panel of seven different MSI-H colorectal cancer PDX models (Extended Data Fig. 6a). Daily treatment with oral dosing of VVD-133214 at 20 mg kg$^{-1}$ was successful at reducing tumour burden in six of the seven models (Fig. 6a,b and Extended Data Fig. 6c–h). CTG-0092 was an exemplary model, with all mice demonstrating tumour regression and three of five mice showing a complete response by study end (Fig. 6b). It is noteworthy that complete responses were observed only in models with p53 mutations (CTG-0092, CTG-0117, CTG-0978), whereas a lower frequency of MSI burden might explain the absence of response in CTG-0067.

The clinical standard of care for MSI-H colorectal cancer is either surgery, chemotherapy (FOLFOX, FOLFIRI or CAPEOX), targeted therapy (anti-vascular endothelial growth factor: bevacizumab, ziv-aflibercept, ramucirumab or anti-epidermal growth factor receptor: cetuximab or panitumumab) or immunotherapy (pembrolizumab or nivolumab)[30]. WRN inhibitors are likely to be used clinically in patients who have failed immunotherapy, and previous work has demonstrated that WRN knockdown is effective in PDX models from patient samples refractory to immunotherapy[31]. We therefore tested VVD-133214 in two different PDX models established from the same patient at different stages of treatment: (1) following surgery and FOLFOX treatment (CTAX-087) and (2) later, following the development of immunotherapy resistance (CTAX-127; Extended Data Fig. 6b). VVD-133214 was effective in both models, with the compound producing an abrupt cessation of tumour growth starting on days 7–10 that persisted until study termination on day 23 (Fig. 6c,d and Extended Data Fig. 6i,j). This profile resulted in tumour growth inhibition of 72–75% for both pre- and postimmunotherapy tumour models, suggesting that VVD-133214 has the potential to suppress tumour growth in patients with MSI-H colorectal cancers that have become resistant to immunotherapy.

## Discussion

The body of work presented here demonstrates the utility of chemoproteomics for discovering and optimizing potent and selective covalent drug candidates against challenging targets like WRN. Careful screening in both cell lysates and live cells, paired with biochemical assays, led to the identification of nucleotide-cooperative WRN inhibitors with a unique covalent allosteric mechanism of action. This class of compounds stabilizes compact conformations of WRN lacking the dynamic flexibility necessary for proper helicase function. Medicinal chemistry optimization furnished VVD-133214, a clinical-stage compound, that precisely recapitulates the phenotype associated with genetic loss of WRN in MSI-H cancer cells, including widespread dsDNA breaks, nuclear swelling, compensatory DNA repair signalling, G2/M cell cycle arrest and cell death. The synthetic lethality of WRN inhibition in MSI-H cancers and the global selectivity of VVD-133214 are supported by the absence of a response in MSS cells and in healthy tissues from mice. Importantly, we found that WRN inhibition maintains synthetic lethality in MSI-H tumour xenografts and PDXs, including in one PDX derived from a patient with a history of resistance to both standard-of-care chemotherapy and checkpoint inhibitors. These findings highlight the potential for WRN inhibition in addressing patients with MSI-H cancer who have a high unmet need. In parallel with our efforts, a separate group recently initiated a clinical trial in patients with MSI-H using a WRN inhibitor[32] and, based on a published patent application[33], that compound appears to be a reversible inhibitor. Together with VVD-133214 (ref. 34), this presents a rare opportunity to compare two small-molecule oncology drugs targeting the same protein by different mechanisms, in the clinic at the same time. Barring clinical development setbacks, this may also offer an opportunity in the future to either sequentially or simultaneously treat patients with both drugs to improve response rates and/or prevent the emergence of drug-specific resistance.

## Online content

Any methods, additional references, Nature Portfolio reporting summaries, source data, extended data, supplementary information, acknowledgements, peer review information; details of author contributions and competing interests; and statements of data and code availability are available at https://doi.org/10.1038/s41586-024-07318-y.


1. Behan, F. M. et al. Prioritization of cancer therapeutic targets using CRISPR-Cas9 screens. *Nature* **568**, 511–516 (2019).
2. Chan, E. M. et al. WRN helicase is a synthetic lethal target in microsatellite unstable cancers. *Nature* **568**, 551–556 (2019).
3. Kategaya, L., Perumal, S. K., Hager, J. H. & Belmont, L. D. Werner syndrome helicase is required for the survival of cancer cells with microsatellite instability. *iScience* **13**, 488–497 (2019).
4. Lieb, S. et al. Werner syndrome helicase is a selective vulnerability of microsatellite instability-high tumor cells. *eLife* **8**, e43333 (2019).
5. van Wietmarschen, N. et al. Repeat expansions confer WRN dependence in microsatellite-unstable cancers. *Nature* **586**, 292–298 (2020).

6. Kawakami, H., Zaanan, A. & Sinicrope, F. A. Microsatellite instability testing and its role in the management of colorectal cancer. *Curr. Treat. Options Oncol.* **16**, 30 (2015).
7. Hause, R. J., Pritchard, C. C., Shendure, J. & Salipante, S. J. Classification and characterization of microsatellite instability across 18 cancer types. *Nat. Med.* **22**, 1342–1350 (2016).
8. Bonneville, R. et al. Landscape of microsatellite instability across 39 cancer types. *JCO Precis. Oncol.* **2017**, PO.17.00073 (2017).
9. Andre, T. et al. Pembrolizumab in microsatellite-instability-high advanced colorectal cancer. *N. Engl. J. Med.* **383**, 2207–2218 (2020).
10. Lenz, H. J. et al. First-line nivolumab plus low-dose ipilimumab for microsatellite instability-Hhigh/mismatch repair-deficient metastatic colorectal cancer: the Phase II CheckMate 142 Study. *J. Clin. Oncol.* **40**, 161–170 (2022).
11. Shan, J., Han, D., Shen, C., Lei, Q. & Zhang, Y. Mechanism and strategies of immunotherapy resistance in colorectal cancer. *Front. Immunol.* **13**, 1016646 (2022).
12. Wang, R. et al. Intrinsic resistance and efficacy of immunotherapy in microsatellite instability-high colorectal cancer: a systematic review and meta-analysis. *Biomol. Biomed.* **23**, 198–208 (2023).
13. Fuca, G. et al. Ascites and resistance to immune checkpoint inhibition in dMMR/MSI-H metastatic colorectal and gastric cancers. *J. Immunother. Cancer* **10**, e004001 (2022).
14. Sui, Q. et al. Inflammation promotes resistance to immune checkpoint inhibitors in high microsatellite instability colorectal cancer. *Nat. Commun.* **13**, 7316 (2022).
15. Huang, S. et al. The premature ageing syndrome protein, WRN, is a 3′->5′ exonuclease. *Nat. Genet.* **20**, 114–116 (1998).
16. Gray, M. D. et al. The Werner syndrome protein is a DNA helicase. *Nat. Genet.* **17**, 100–103 (1997).
17. Zong, D. et al. Comprehensive mapping of cell fates in microsatellite unstable cancer cells support dual targeting of WRN and ATR. *Genes Dev.* **37**, 913–928 (2023).
18. Backus, K. M. et al. Proteome-wide covalent ligand discovery in native biological systems. *Nature* **534**, 570–574 (2016).
19. Weerapana, E. et al. Quantitative reactivity profiling predicts functional cysteines in proteomes. *Nature* **468**, 790–795 (2010).
20. Parker, M. J. et al. Identification of 2-sulfonyl/sulfonamide pyrimidines as covalent inhibitors of WRN using a multiplexed high-throughput screening assay. *Biochemistry* **62**, 2147–2160 (2023).
21. Hansen, R. et al. The reactivity-driven biochemical mechanism of covalent KRASG12C inhibitors. *Nat. Struct. Mol. Biol.* **25**, 454–462 (2018).
22. Rudolph, M. G. & Klostermeier, D. When core competence is not enough: functional interplay of the DEAD-box helicase core with ancillary domains and auxiliary factors in RNA binding and unwinding. *Biol. Chem.* **396**, 849–865 (2015).
23. Cancer Dependency Map Portal (RRID:SCR_017655). *DepMap Portal* https://depmap.org/portal/ (2019).
24. Bird, J. L. et al. Recapitulation of Werner syndrome sensitivity to camptothecin by limited knockdown of the WRN helicase/exonuclease. *Biogerontology* **13**, 49–62 (2012).
25. Soto-Gamez, A., Quax, W. J. & Demaria, M. Regulation of survival networks in senescent cells: from mechanisms to interventions. *J. Mol. Biol.* **431**, 2629–2643 (2019).
26. Kang, K., Lee, S. B., Yoo, J. H. & Nho, C. W. Flow cytometric fluorescence pulse width analysis of etoposide-induced nuclear enlargement in HCT116 cells. *Biotechnol. Lett.* **32**, 1045–1052 (2010).
27. Skog, S. & Tribukait, B. Cell size following irradiation in relation to cell cycle. *Acta Radiol. Oncol.* **25**, 269–273 (1986).
28. Rogakou, E. P., Pilch, D. R., Orr, A. H., Ivanova, V. S. & Bonner, W. M. DNA double-stranded breaks induce histone H2AX phosphorylation on serine 139. *J. Biol. Chem.* **273**, 5858–5868 (1998).
29. Liu, Y. et al. Patient-derived xenograft models in cancer therapy: technologies and applications. *Signal Transduct. Target. Ther.* **8**, 160 (2023).
30. Overman, M. J. Overview of the management of primary colon cancer. *uptodate* https://www.uptodate.com/contents/overview-of-the-management-of-primary-colon-cancer (2024).
31. Picco, G. et al. Werner helicase is a synthetic-lethal vulnerability in mismatch repair-deficient colorectal cancer refractory to targeted therapies, chemotherapy, and immunotherapy. *Cancer Discov.* **11**, 1923–1937 (2021).
32. *Study of HRO761 Alone or in Combination in Cancer Patients With Specific DNA Alterations Called Microsatellite Instability or Mismatch Repair Deficiency* (US National Library of Medicine, 2023): https://classic.clinicaltrials.gov/show/NCT05838768.
33. Bordas, V. et al. Triazolo-pyrimidine analogues for treating diseases connected to the inhibiton of Werner syndrome RECQ helicase (WRN). International Patent WO 2022/249060 (2022).
34. *A Study to Evaluate the Safety, Pharmacokinetics, and Anti-tumor Activity of RO7589831 in Participants with Advanced Solid Tumors* (US National Library of Medicine, 2023); https://classic.clinicaltrials.gov/show/NCT06004245.
35. Newman, J. A. et al. Crystal structure of the Bloom's syndrome helicase indicates a role for the HRDC domain in conformational changes. *Nucleic Acids Res.* **43**, 5221–5235 (2015).

# Methods

### Compounds

VVD-133214 (also referred to as RO7589831) has a molecular weight of 437.46 g $mol^{-1}$ and was synthesized at WuXi (China); all batches had a purity of over 99%. VVD-133214, etoposide (MP Biomedicals, catalogue no. ICN19391883) and navitoclax (Selleck Chemical LLC, catalogue no. 50-849-6) were stored in DMSO in 10 mM aliquots at room temperature.

### Cell lines

Cell lines HCT-116 (ATCC, no. CCL-228), LoVo (ATCC, no. CCL-229), RKO (ATCC, no. CRL-2577), SW48 (ATCC, no. CCL-231) and DLD-1 (ATCC, no. CCL-221) and SW480 tumour cells (ATCC, no. CCL-228) were authenticated at ATCC using the short tandem repeat (STR) method, cultured according to the manufacturer's instructions and routinely tested for mycoplasma. WRN C727 mutant HCT-116 cells were generated by electroporation with Cas9 nuclease (Integrated DNA Technologies (IDT), no.1081059), CRISPR–Cas9 transactivating CRISPR RNA (IDT, no. 1072532) prehybridized to a CRISPR RNA (crRNA) targeting the genomic region near the codon translating to C727 of the *WRN* gene, and a 100 base pair DNA donor oligo spanning around 50 base pairs upstream and downstream of the C727-encoding codon. Nucleofection was completed using Lonza P3 Primary Cell 4D-Nucleofector X Kit S (Lonza, no. V4XP-3032). The crRNA was designed using the CHOPCHOP database (https://chopchop.cbu.uib.no/). Individual cell clones were generated by limiting dilution and confirmed for C727A knock-in by Sanger sequencing. An individual mutant clone with comparable WRN expression and growth rate was selected for expansion.

### In vitro target engagement assays

HCT-116, OCI-AML2, SW480 and DLD-1 cell pellets were lysed by probe sonication in 20 ml of 1× Gibco DPBS. Protein concentration was normalized with 500 µg of total protein aliquot to each well of a 96-well plate. Lysates were treated with compound for 1 h and solvent-exposed cysteines were labelled by the addition of an IAA probe (custom synthesis, WuXi App Tec) for 1 h. Samples were treated with benzonase nuclease (Millipore Sigma, catalogue no. 70746-3) before acetone precipitation. Precipitated protein was resuspended in freshly made buffer (9 M urea, 50 mM ammonium bicarbonate, 10 mM dithiothreitol (DTT)). Samples were alkylated with IAA and desalted with Zeba desalting plates (Thermo Fisher Scientific, catalogue no. 89807). Following digestion, cysteine-containing peptides were captured using 5% high-capacity streptavidin agarose. Eluted peptides were dried and resuspended in 3% acetonitrile and 0.1% formic acid for mass spectrometry analysis. Engagement (at a given concentration) was measured twice (technical replicates) across a five-point $TE_{50}$ curve. $TE_{50}$ values were derived from a single experiment for many compounds depicted in scatter plot graphs, whereas those for certain high-interest compounds were derived from the average of multiple independent experiments.

### Liquid chromatography–tandem mass spectrometry analysis

Probe-labelled peptides were concentrated onto an Acclaim PepMap100 C18 loading column (Thermo Fisher Scientific, catalogue no. DX164564; 100 µm × 2 cm, 5 µm particle size) and separated on a custom-made C18 nanoviper analytical column (75 µm × 15 cm, 2 µm particle size) using a Dionex Ultimate 3000 nanoliquid chromatography apparatus (Thermo Fisher Scientific). Peptides were separated using a 12.7 min gradient from 6 to 32.5% solvent B (96.4% acetonitrile, 3.5% DMSO (Pierce, catalogue no. 20688) and 0.1% formic acid) mixed with solvent B (96.4% water, 3.5% DMSO, 0.1% formic acid). Peptides were analysed by parallel reaction monitoring (PRM) mass spectrometry using product ion scan mode on a Thermo Exploris 120 orbitrap mass spectrometer. Precursor ions were fragmented and measured using a normalized collision energy of 25%, 0.7 *m/z* Q1 resolution, 30,000 orbitrap resolution, 70% reimagined focus lens and customized normalized automatic gain control target (percentage) in positive-polarity mode. This was a scheduled method, with 1.2 min windows and dynamic injection time mode with a minimum of seven points across the peak.

Target engagement (WRN C727) was measured by monitoring the peptide NPQITC*TGFDRPNLYLEVR (854.1162 *m/z*). Additional peptides were measured to quantify total WRN protein levels, in addition to other peptides not impacted by WRN inhibition, to ensure that only WRN inhibition-related peptides had changed. Retention time standard peptides were also included in the method and were used for global normalization.

Mass spectrometry data were analysed using a Skyline V21.2.0.369 (MacCoss Lab, University of Washington). Peptide quantification was performed by summing of peak areas corresponding to between three and six fragment ions, which were preselected from a reference spectral library. Endogenous reference peptides were used to normalize for sample variability. Percentage target engagement for each peptide was determined by comparison of average peptide AUC obtained from each compound-exposed sample with that of the control (DMSO-exposed) sample. Target engagement was measured as a loss of the C727-containing peptide signal.

### In vitro determination of WRN protein half-life

HCT-116 cells were passaged at least twice in RPMI medium (Thermo Fisher Scientific, catalogue no. 88365) with 10% dialysed fetal bovine serum (Thermo Fisher Scientific, catalogue no. 26400044) and prepared for stable isotope labelling by amino acids in cell culture supplemented with light L-arginine (Sigma-Aldrich, catalogue no. L5501-5G) and L-lysine (Sigma-Aldrich, catalogue no. L5501-5G). Cells were split 1:4 from an 80% confluent flask into four new flasks for assessment at 0, 2, 6 and 24 h. Heavy stable isotope labelling by amino acid RPMI, supplemented with 10% dialysed fetal bovine serum, heavy L-arginine (+10 Da, FW 220.59; Sigma-Aldrich, catalogue no. 608033) and heavy L-lysine (+8 Da, FW 190.59; Sigma-Aldrich, catalogue no. 608041), was first added to the 24 h flask and, the following day, to the 2 and 6 h flasks to synchronize cell harvesting. Light medium was decanted and cells were rinsed with Gibco DPBS (catalogue no. 14190-136) before changing the medium. Cells were detached from the plate using TrypLE Express Enzyme (Thermo Fisher Scientific, catalogue no. 12605010) and centrifuged at 500*g* for 5 min. Trypsinized cells were washed twice with PBS and cell pellets stored at −80 °C until processing. Lysates were processed as described for chemoproteomic analysis with cysteine probe enrichment and measured by PRM. The heavy-labelled and endogenous versions of the following WRN peptides were used to determine the level of heavy amino acid incorporation, which is used to calculate WRN half-life: ANTESQSLILQANEELCPK (1206.6256 and 1210.6327 *m/z*), LYSYKPCDK (480.9234 and 486.2662 *m/z*), CAVEER (515.771 and 520.7752 *m/z*), SLCFQYPPVYVGK (912.9895 and 916.9966 *m/z*) and NPQITCTGFDRPNLYLEVR (854.1162 and 860.7884 *m/z*). WRN half-life was determined by first calculating protein decay rate ($K_{dp}$) and then applying the formula $T_{1/2} = \log_e 2/K_{dp}$ (ref. 36).

### Helicase activity assay

The helicase assay was adapted from a published protocol[37]. Human WRN constructs (ATPase domain) ($hWRN^{532–948}$ C946S), Helicase Core ($hWRN^{519–1093}$), Helicase Core w/ HRDC ($hWRN^{519–1227}$) or Full Length (1–1,432), C727A-mutant hWRN ($hWRN\ C727A^{519–1245}$), human BLM (hBLM) ($hBLM^{636–1298}$) or mouse WRN (mWRN, WT $mWRN^{486–1232}$) were diluted in assay buffer (50 mM Tris-HCl pH 7.5, 2 mM $MgCl_2$, 100 mM NaCl, 0.01% Tween-20, 0.0025 U $ml^{-1}$ poly deoxyinosinic-deoxycytidylic acid sodium salt, 0.003% bovine serum albumin (BSA), 1 mM DTT), with or without 0.2 mM ATP and with or without 1 mM DTT, and plated in the assay plate (10 µl per well). Proteins were preincubated with VVD-133214 (11-point dose–response, 0–50 µM, threefold serial dilutions, 0.5% DMSO) at room

temperature for 30 min. The reaction was initiated by the addition of a 10 µl per well mixture containing ATP, the DNA-capturing strand (GAACGAACACATCGGGTACG) and the TAMRA-labelled DNA duplex DNA OLIGOA-BHQ2: TTTTTTTTTTTTTTTTTTTTTTTTTTTTTTTTTTC GTACCCGATGTGTTCGTTC/BHQ2, OLIGOB-TAMRA: TAMRA/GA ACGAACACATCGGGTACGTTTTTTTTTTTTTTTTTTTTTTTTTTTTTT. After 30 min, endpoint measurement of fluorescence was performed (ex./em. 535/585 nm, CLARIOstar (BMG Labtech)). Activity was normalized to no-enzyme negative controls (0%) and to DMSO-treated positive control (100%). The reference compound NSC 617145 (Tocris, no. 5340), a non-specific helicase inhibitor, was used as a control for inhibition. Unless otherwise specified, all results were derived from a representative experiment with two technical replicates.

### WRN ATPase activity assay

WT hWRN (hWRN$^{519–1227}$) was diluted in assay buffer (50 mM Tris-HCl pH 7.5, 2 mM $MgCl_2$, 100 mM NaCl, 0.01% Tween-20, 0.0025 U $ml^{-1}$ poly deoxyinosinic-deoxycytidylic acid sodium salt, 0.003% BSA, 1 mM DTT) with or without 50 µM ADP and plated in the assay plate (10 µl per well). WRN was preincubated with VVD-133214 (11-point dose–response, 0–50 µM, threefold serial dilutions, 0.5% DMSO) at room temperature for 30 min. The reaction was initiated by the addition of a 10 µl per well mixture containing ATP with or without the DNA-capturing strand (GAACGAACACATCGGGTACG) and the TAMRA-labelled DNA duplex DNA. After 30 min the reaction was quenched with the addition of Biomol Green (Fisher, no. NC0007114) with 10 µM EDTA, incubated for 15 min at room temperature and an endpoint measurement of absorbance at 630 nm was performed (CLARIOstar, BMG Labtech). Activity was normalized to no-enzyme negative controls (0%) and to DMSO-treated positive control (100%).

### WRN DNA HTRF assay

WT hWRN (hWRN$^{519–1227}$) was diluted with assay buffer (50 mM Tris-HCl pH 7.5, 2 mM $MgCl_2$, 100 mM NaCl, 0.01% Tween-20) with or without 50 µM ADP and plated in the assay plate (10 µl per well). Protein was then preincubated with either VVD-133214 (11-point dose–response, 0–50 µM, threefold serial dilutions, 0.5% DMSO) at room temperature for 30 min. The reaction was initiated by the addition of a 10 µl per well mixture containing biotinylated duplex DNA OLIGOA-BHQ2: TTTTTTTTTTTTTTTTTTTTTTTTTTTTTTTTCGTACCCGATGTGTTCGT TC, OLIGOB-biotin: TAMRA/GAACGAACACATCGGGTACGTTTTTT TTTTTTTTTTTTTTTTTTTTTTT. The final concentrations of WRN and biotinylated DNA were 5 and 20 nM, respectively. After 30 min, endpoint measurement of homogenous time-resolved fluorescence (HTRF) was performed (Pherostar, BMG Labtech). Activity was normalized to no-enzyme negative controls (0%) and to DMSO-treated positive control (100%).

### Recombinant protein expression and purification

Human WRN (residues 517–945 for crystallization and 519–1,227 for biochemical experiments) and mouse WRN (486–1,232) were fused to a C-terminal prescission-cleavable GFP-8xHis tag. The C727A variant of human WRN was expressed as for an N-terminal 8xHis-SUMO fusion with a TEV cleavage site. All WRN constructs synthesized and cloned at Genscript were expressed recombinantly in Sf9 insect cells. All constructs were purified in a similar manner using the following steps, all performed at 4 °C. Briefly, cells were suspended in 50 mM Tris/HCl pH 8.5, 2 M NaCl, 0.5 mM TCEP, 10 mM $MgCl_2$, 5% (v/v) glycerol and 5 mM ADP supplemented with protease inhibitors, diisopropyl fluorophosphates and Benzonase, and were disrupted in a microfluidizer. Protein was bound to $Ni^{2+}$-NTA His Bind Superflowresin followed by cleavage of the GFP tag with HRV 3 C protease in 50 mM Tris/HCl pH 7.0, 0.35 M NaCl, 0.5 mM TCEP, 5% (v/v) glycerol and ion exchange chromatography on either a ToyoScreen sulfate-650F or heparin column, with final size exclusion on a Superdex S200 column in 20 mM Tris/HCl pH 7.5, 350 mM NaCl, 0.25 mM TCEP and 2.5% glycerol. Human Bloom helicase (hBLM$^{636–1298}$_N-6His-SUMO-Avi-TEV) was expressed in *Escherichia coli* and purified as outlined below. Briefly, cells were suspended in 50 mM Tris/HCl pH 8.0, 2 M NaCl, 2 mM TCEP, 10 mM $MgCl_2$, 10% (v/v) glycerol and 20 mM imidazole, supplemented with Roche EDTA-free tablets (1/50 ml) and Benzonase 1:10,000 and disrupted in a microfluidizer. Protein was bound to a HisTrap column following washing of bound protein with reduced NaCl (300 mM) in the presence of 0.35% Chaps; protein was then eluted in an imidazole gradient and pooled fractions cleaved with SUMO-protease overnight at 4 °C. Following concentration, final size exclusion was performed on a S200 HiLoad column in 20 mM Tris/HCl pH 8.0, 300 mM NaCl, 2 mM TCEP and 10% glycerol.

### Crystallization, data collection and structure determination

Protein solution was prepared by mixing 44 µM WRN$^{517–945}$ with final concentrations of 3 mM ADP and 6 mM $MgCl_2$ with or without threefold molar excess of inhibitor. Following incubation for 60 min, the complex was concentrated using an Amicon Ultra-4 centrifugation unit (Merck Millipore, 30 MWCO, RC) to a final concentration of 100 µM. Crystals of the hWRN$^{517–945}$–inhibitor complex were obtained after 4 days at 293 K in the sitting drop vapour diffusion format by mixing 0.1 µl of protein solution, 0.08 µl of reservoir solution and 0.02 µl of seed solution. The best-diffracting complex crystals were crystallized from 20% (w/v) PEG 3350, 0.2 M $NaNO_3$ and 0.1 M Bis-Tris propane/NaOH pH 6.5 (crystals were also obtained under other conditions with anions and over the pH range 6.5–8.5). The best-diffracting crystals of hWRN$^{517–945}$ with ADP were obtained after 1 day at 277 K in the sitting drop vapour diffusion format by mixing 0.14 µl of protein solution, 0.04 µl of reservoir solution and 0.02 µl of seed solution. The reservoir solution comprised 2.7% (v/v) Jeffamine T-403, 13.6% (v/v) pentaerythritol ethoxylate (15/4 EO/OH), 0.18 M potassium acetate, 0.4 mM $CdCl_2$, 0.4 mM $CoCl_2$, 0.4 mM $CuCl_2$, 0.4 mM $NiCl_2$, 2 mM HEPES/HCl pH 6.8 and 91 mM MES/NaOH pH 6.0 (crystals were also obtained under other conditions and at 293 K). Crystals of hWRN$^{517–945}$ with ATP were obtained after 1 day at 277 K in the sitting drop vapour diffusion format by mixing 0.11 µl of protein solution, 0.02 µl of reservoir solution and 0.02 µl of seed solution, and were crystallized from 10% (w/v) PEG 8000, 0.2 M NaCl and 0.1 M sodium/potassium phosphate pH 6.2. Seeds were always prepared using Seed Beads with hWRN$^{517–945}$ crystals grown in 20% (v/v) ethylene glycol, 11% (w/v) PEG 8000, 80 mM MES/NaOH pH 6.5 and 80 mM imidazole. Initial crystals for seeding grew at 277 K from 15% (v/v) pentaerythritol ethoxylate (15/4 EO/OH), 3% (v/v) Jeffamine T-403, 0.2 M KOAc and 0.1 M MES/NaOH pH 6.0. Crystals were dipped in paraffin oil and vitrified by hyperquenching in liquid nitrogen.

Data were collected from a single crystal per complex at 100 K at the Swiss Light Source beamline PX-II on an EIGER2-16M detector with X-rays of 1 Å wavelength and 0.25° oscillation. Intensities were integrated with XDS, scaled with AIMLESS and treated for anisotropy using STARANISO (GlobalPhasing, Ltd). High-resolution limits for data were selected based on signal to noise ($I/\sigma(I) \geq 1$) and correlation coefficient at half-dataset ($CC_{1/2}$) ≥ 0.3 in the outer shell. Phases were generated by molecular replacement with PHASER using an in-house WRN search model without ligand. Models were rebuilt in Coot and refined with Phenix using individual and TLS (translation, libration, screw-rotation) protocols for B values. Weights for B values, protein geometry and bulk solvent mask were optimized automatically during refinement. The final structures contained one molecule per asymmetric unit. Data collection and refinement statistics were calculated using phenix.table_one (Extended Data Table 2), with standard distributions for Ramachandran and Molprobity assessment taken from the Top8000 database of high-resolution protein structures. Pymol was used to superimpose coordinates and render figures. The VVD-133214/ADP (7GQU), ATP (7GQT) and ADP (7GQS) structures have 97.8, 97.8 and 98.1%, respectively, of all residues in the favoured regions of the Ramachandran plot, with the remainder in the allowed regions.

No Ramachandran outliers were present in any of the three crystal structures. Pymol was used to superimpose coordinates and render figures.

### Intact protein mass spectrometry and rate determination

To observe covalent ligand engagement of recombinant WRN, samples were analysed following formic acid quenching on an Agilent LC1290 Infinity II instrument coupled to a 6545 QTOF liquid chromatography–mass spectrometer (Agilent Technologies). A sample volume of 15 µl, equivalent to approximately 1.5 pmol of WRN protein, was injected. The protein was desalted and separated on an AERIS 3.6-µM-wide-bore XB-C8 liquid chromatography column (50 × 2.1 $mm^2$, Phenomenex) at 60 °C at a flow rate of 0.5 ml $min^{-1}$. Liquid chromatography solvent A comprised 0.1% formic acid in 99.9% water, and solvent B was 0.1% formic acid in 99.9% acetonitrile. The column was equilibrated in 10% B for 30 s, followed by a 3.5 min gradient from 10 to 70% B to separate the analytes. This was followed by a 15 s gradient from 70 to 95% B, a 15 s gradient from 95 to 10% B, a 15 s gradient from 10 to 95% B and finally a 15 s gradient from 95 to 10% B to clean the column before re-equilibration. Mass spectra were acquired from 700 to 1,700 Da at a resolution of 25,000. A Dual Agilent Jet Stream Electrospray Ionization Source was used for ionization. The gas temperature was set to 325 °C, with a flow rate of 10 l $min^{-1}$. The nebulizer was set to 45 pounds per square inch and sheath gas temperature and flow were set to 375 °C and 12 l $min^{-1}$, respectively. One spectrum was acquired per second with a collision energy of 10 V. The capillary voltage was set to 5,000 V and the nozzle voltage to 2,000 V. The fragmenter, skimmer and octopole radio frequency (RF) peaks were set at 250, 65 and 750 V, respectively. The resulting data files were deconvoluted to protein masses using Agilent MassHunter BioConfirm Software, v.11.0. The biomolecule table containing protein mass and peak intensities was used to quantify the percentage of compound modification relative to the unmodified protein peak, by dividing modified protein intensity by the sum of the unmodified and modified protein intensities. $k_{obs}/[I]$ was calculated using assumptions for pseudo-first-order reaction kinetics (d(VVD-133214)/d$t$ = $-k$ × (VVD-133214), $(\text{VVD-133214})_t = (\text{VVD-133214})_{t0} \times e^{-kt}$) and averaged for each inhibitor concentration; $k_{obs}$ was determined by dividing these values by ($I$) for each concentration.

### GSH reactivity assay

In brief, glutathione (GSH) was diluted to a final concentration of 50 µM in buffer comprising 0.1 M Tris pH 8.8 and 30% acetonitrile. In triplicate, 100 µl of GSH solution was added to a clear 384-well plate (Greiner, no. 781101). Next, 5 µl of 10 mM electrophilic compounds was added to the GSH solution to achieve a final concentration of 500 µM and the reaction was incubated for the 2 and 6 h time points at room temperature; 5 µl of 100 mM Ellman's reagent was then added to the plate and absorbance read at 440 nm. The concentration of GSH remaining was derived from a standard curve, and observed rate ($k_{obs}/(I)$) was calculated assuming pseudo-first-order reaction kinetics from the following equations: d(GSH)/d$t$ = $-k$ × (GSH), $(\text{GSH})_t = (\text{GSH})_{t0} \times e^{-kt}$).

### CTG assay

HCT-116, SW480 and HCT-116 WRN C727A mutant cells were seeded overnight in 384-well plates at 500–1,000 cells per well in complete media. Compound dilutions were then added to the remaining cells in a 1:3, ten-point dose–response format starting at 100 µM. At the end of the 5 day incubation period, CTG 2.0 reagent was added to each well. Luminescence was read on a Clariostar plate reader (BMG Labtech).

Relative growth was calculated by normalizing the growth of compound-treated cells to that of DMSO-treated cells using the following equation: (treatment $t_5 - t_0$)/(DMSO $t_5 - t_{0)}$) × 100, where $t_5$ represents cell viability after 5 days of treatment and $t_0$ represents cell viability before treatment. The concentrations required to reach $GI_{50}$ and $GI_{MAX}$ are reported. Unless otherwise specified, all figures were derived from a representative experiment with two technical replicates.

### High-content nuclear count assay

All experiments were initiated by seeding HCT-116, SW48, LoVo and SW480 cells in a 384-well plate at 3,000 cells per well in complete media. Cells were incubated with either (1) VVD-133214 dilutions in a ½ log, ten-point dose–response format starting at 20 µM, in duplicate, at 37 °C and 5% $CO_2$ for 5 days; (2) 2 µM VVD-133214 at 37 °C and 5% $CO_2$ for 2, 4, 6, 9, 12, 16, 19, 23, 30 or 37 days; or (3) 2 µM VVD-133214 at 37 °C and 5% $CO_2$ for 2, 8, 24, 48 or 72 h, then washed twice with the appropriate medium and then were allowed to grow for the remainder of the 144 h time point in the absence of VVD-133214. Cells were fixed with room-temperature (25 °C) methanol for 5 min. The wells were then washed twice with PBS and incubated with Hoechst 33342 (Thermo Fisher Scientific, catalogue no. 62249), diluted 1:5,000 in PBS + 0.1% Tween-20 at room temperature for 5 min and fluorescence was read on an Operetta CLS (PerkinElmer). Fixed-time point, dose–response experiments were run with four technical replicates; time course experiments were run with eight technical replicates.

### Comet assay

SW48 cells ($3\times 10^5$) were treated with 1 µM VVD-133214 for 48 h in a 12-well dish. Cells were harvested with TrypLE (Thermo Fisher Scientific, no. 12605019) and resuspended to $1\times 10^5$ cells $ml^{-1}$ in PBS. This was followed by 1:10 dilution in low-melting-point agarose, with 50 µl spotted onto the comet slide (R&D Systems, no. 4250-050-K). Agarose was polymerized at 4 °C for 10 min, followed by 30 min incubation in ice-cold lysis solution. Slides were then electrophoresed in ice-cold 0.5 M Tris (Thermo Fisher Scientific, no. 17926) and 1.5 M sodium acetate (Thermo Fisher Scientific, no. J66397.36) for 40 min at 21 V. DNA was precipitated ar room temperature in 70% ethanol and 300 mM ammonium acetate (Thermo Fisher Scientific, no. AM9071) for 5 min. Slides were dried at 37 °C for 20 min, followed by the addition of 1× SYBR-Gold (Thermo Fisher Scientific, no. S11494). Images were acquired on an Operetta CLS (Alexa 488 channel). Figures depict a single representative run.

### Metaphase spreads

Metaphase spreads were performed on SW48 cells as previously described[5]. Briefly, following 42 h incubation with 125 nM VVD-133214, cells were treated with 1.5 µM nocadozole and 1 mM caffeine for 6 h. Cells were trypsinized, washed in PBS and placed in a prewarmed, hypotonic 50 mM KCl solution supplemented with 15 mM HEPES for 30 min at 37 °C. Before cell pelleting, 1 ml of ice-cold Carnoy's solution (3:1, MeOH:AcOH) was added to the KCl solution to stabilize metaphase spreads. Samples were then resuspended and fixed in 10 ml of ice-cold Carnoy's solution for 1 h at room temperature. Cell suspensions were dropped from a height of approximately 60 cm onto slides, stained with Hoechst 33342, mounted in Invitrogen ProLong Gold antifade reagent (catalogue no. P36934) and visualized with a TissueFAXS SL Slide Scanner (TissueGnostics). Images were captured at ×100. Figures depict a single representative run.

### Phospho-H2AX immunofluorescence

HCT-116, RKO or SW480 cells were seeded on 384-well plates at 2,500–20,000 cells per well for incubation with VVD-133214 in a dose–response format starting at either 10 or 20 µM. Cells were fixed and permeabilized with 60 µl of ice-cold 100% methanol. They were then visualized with anti-phospho-H2AX antibody (1:50; Novus Biologics, catalogue no. NB100-74435) and goat anti-mouse secondary antibody conjugated to Alexa Fluor 488 (1:50; Thermo Fisher Scientific, catalogue no. A-32723), and nuclei were visualized with Hoechst 33342. Fluorescence was read on an Operetta CLS apparatus (PerkinElmer). Experiments were conducted with two technical replicates, with graphs depicting a single representative run.

### Simple Western immunoblotting

HCT-116, LoVo or SW480 cells were seeded at 100,000 cells per well on 96-well, tissue culture-treated plates. VVD-133214 was then either (1) added to cells at 2 μM for 2, 8, 24, 48 or 72 h or (2) used in a five-point-dilution dose–response format starting at 4 μM for 24 h. Cells were lysed in Pierce IP lysis buffer (Thermo Fisher Scientific, catalogue no. 87788) containing HALT protease and phosphatase inhibitor cocktail (1:100; Thermo Fisher Scientific, catalogue no. 78446), 1 mM $MgSO_4$ (Sigma-Aldrich, catalogue no. M2643) and benzonase nuclease (1:100; Millipore Sigma, catalogue no. 70746). Protein concentration was determined using a Pierce bicinchoninic acid (BCA) protein assay kit (Thermo Fisher Scientific, catalogue no. 23227). Protein content was then normalized to 1.0 μg $\mu l^{-1}$ in Pierce IP lysis buffer. Normalized samples were used for Simple Western analysis using the Jess instrument (Bio-techne, Protein Simple, Inc.) according to the user guide for Jess (P/N PL2-0004, Revision F). Samples were immunoblotted with either anti-WRN (1:50; Cell Signaling Technology, catalogue no. CST4666), anti-p53 (1:50; Cell Signaling Technology, catalogue no. 9282), anti-phospho-p53 (1:50; Cell Signaling Technology, catalogue no. 9284 T), anti-α-tubulin (1:50; Cell Signaling Technology, catalogue no. 2125 T) or anti-p21 (1:50; abcam, catalogue no. ab109520). The secondary antibody was provided in either the Anti-Rabbit Detection Module Chemiluminescence package (Bio-Techne, catalogue no. DM-001) or the Anti-Mouse Detection Module Chemiluminescence package (Bio-Techne, catalogue no. DM-002). In vitro Simple Western figures and quantitative graphs depict a single representative experiment, with each lane representing a single concentration of compound.

### Cell cycle and flow cytometry

HCT-116, SW48 or SW480 ($2 \times 10^6$) cells were seeded on 10 cm plates in 10 ml of medium and allowed to adhere at 37 °C and 5% $CO_2$ overnight. Cells were incubated with either 2 μM VVD-133214 (24, 48 or 72 h), 2 μM etoposide (24 h) or DMSO (24 h). For compound dose–response experiments, SW48 cells were incubated with either DMSO, 2 μM etoposide or twofold serial dilutions of VVD-133214 in an eight-point, dose–response format starting at 2 μM for 48 h. Cells were incubated with 10 μM EdU (Invitrogen, catalogue no. A10044) at 37 °C and 5% $CO_2$ for 2 h before harvesting.

Cells were harvested by trypsinization, washed, fixed in BD CytoFix Fixation Buffer (Thermo Fisher Scientific, catalogue no. 554655) for 15 min, resuspended in 1 ml of 1% BSA in 1× PBS and stored at 4 °C until all samples were collected.

A Click reaction cocktail was prepared according to calculations from the Click-iT Plus Alexa Fluor 488 Picolyl Azide Toolkit (Invitrogen, catalogue no. C10461). Samples were incubated in reaction cocktail at 25 °C away from light for 30 min and then pelleted at 3,000 rpm for 1 min. Supernatants were discarded and samples washed twice in 1% BSA and 0.1% Triton X-100 in 1× PBS. After washing, samples were resuspended in 100 μl of 1% BSA and 0.1% Triton X-100 in 1× PBS supplemented with phospho-Histone H3 (Ser10) rabbit monoclonal antibody (Alexa Fluor 647 Conjugate; Cell Signaling Technology, catalogue no. 3458) at a dilution of 1:100.

Samples were incubated at 25 °C away from light for 45 min and then pelleted at 3,000 rpm for 1 min. After discarding supernatants, cells were washed twice in 1% BSA and 0.1% Triton X-100 in 1× PBS and resuspended in 100 μl of 1% BSA and 0.1% Triton X-100 in 1× PBS supplemented with FxCycle Violet stain (Invitrogen, catalogue no. F10347) at a dilution of 1:1,000. Samples were incubated at 25 °C away from light for 30 min and then analysed on a Beckman Coulter Cytoflex S flow cytometer using the following laser gain settings: forward scatter 10, side scatter 10, Pacific Blue Dye, V450 (no. PB450) 10, fluorescein isothiocyanate 20, allophycocyanin 300. All flow cytometry data were analysed by FlowJo software (v.10.8.1). The gating strategy for flow cytometry analysis determining DNA content, EdU incorporation and phospho-Histone H3 (Ser10) is outlined in Extended Data Fig. 3k. Experiments quantitating DNA content, run with two technical replicates and 20,000 cells, were analysed per sample per experiment. Graphs depicting EdU labelling and phospho-histone H3 (Ser10) staining depict a single sample per time point.

### Apoptosis assay

HCT-116 and SW480 cells at 500 per well were plated in 384-well plates (Thermo Fisher Scientific, catalogue no. NC1758152). Cells were dosed with serial dilutions of either VVD-133214 or navitoclax in the presence of bioluminescent annexin V detection reagent (Promegas, catalogue no. JA1012). The assays were performed with compound incubation for 24, 48 or 72 h according to the manufacturer's instructions. Experiments were conducted with two technical replicates, with graphs depicting a single representative run that included assessments at different time points.

### Animal studies

Five-week-old female homozygous Foxn1 <nu> mice were obtained from Jackson Laboratories (catalogue no. 007850). Animals were housed in Innovive disposable cages prefilled with sterile corncob or ALPHA-dri bedding. Animals were provided ad libitum access to irradiated Envigo Teklad 18% soy Rodent Diet 2920X and to prefilled, sterilized water bottles. Mice were maintained on a 12/12 h light/dark cycle with room temperature at 24 ± 3 °C and ambient relative humidity. Animals were maintained in accordance with the guidelines for the care and use of laboratory animals as approved by the appropriate Institutional Animal Care and Use Committees. All animal procedures were conducted in a facility accredited by the Association for Assessment and Accreditation of Laboratory Animal Care. Studies were run at Vividion, HD Bioscience (San Diego, CA) and Champions Oncology (Rockville, MD) (PDX models) and at the Autonomous University of Barcelona. A maximum tumour size of 2,000 $mm^3$ was permitted.

Following the acclimation period (3–7 days), each animal was inoculated subcutaneously in the right lower flank with $10^7$ tumour cells of 95% or greater viability in a 1:1 mix of PBS and Matrigel (1:1 v/v; Corning, catalogue no. 356237). Animals were randomized into treatment groups ($n$ = 4–8 per group) based on tumour size, with a mean of roughly 150 $mm^3$ for randomization across all studies. Studies were not blinded. The start of the study, where randomization and dosing began, was designated as Day 0.

VVD-133214 was formulated in 10% *N*-methyl-2-pyrrolidinone, 15% Kolliphor EL, 1% Tween-20 and 14.8% hydroxy-propyl-beta-cyclodextrin at a concentration of 2 mg $ml^{-1}$. Mice were dosed orally via gavage with either vehicle or VVD-133214 at 10 ml $kg^{-1}$, once daily for the study duration. Tumour measurements and body weights were obtained twice weekly. Tumour size was measured in two dimensions using a digital caliper, with volume expressed in cubic millimetres using the formula $V(mm^3) = (a \times b^2)/2$, where $a$ and $b$ are the long and short diameters of the tumour, respectively.

Following 2–6 weeks of treatment with either VVD-133214 or vehicle, 150 μl of blood was collected under isoflurane anaesthesia via the saphenous vein 30 min after the last dose, or terminal blood was collected by cardiocentesis 2 h after the last dose; plasma, tumour and spleen were frozen at −80 °C for further analysis.

### In vivo sample preparation

Samples were lysed using Pierce radioimmunoprecipitation (RIPA) buffer (Thermo Fisher Scientific, catalogue no. 89900) containing HALT protease and phosphatase inhibitor cocktail, 1 mM $MgSO_4$ and benzonase nuclease, and homogenized using a Bead Mill homogenizer (OMNI International, SKU 19-042E). Following homogenization, samples were centrifuged at 4,000*g* and 4 °C for 10 min. Following pelleting of insoluble materials, supernatant was collected and protein concentration determined using the Pierce BCA protein assay kit. The final

total protein concentration in each sample was normalized to 1 mg $ml^{-1}$ using RIPA lysis buffer and was confirmed by BCA assay. Normalized samples were used for Simple Western analysis using either the Jess instrument (Bio-techne) or mass spectrometry target engagement.

### In vivo target engagement

Target engagement (WRN_C691) in the spleen was measured by monitoring peptide DPQIT**C**TGFDRPNLYLEVGRK (916.1497 *m/z*). Additional peptides were measured to quantify total WRN, p21 and p53 protein levels in the tumour, in addition to measurement of other peptides not impacted by WRN inhibition, to ensure that only WRN inhibition-related peptides changed. Peak areas (AUCs) were quantified by integrating the peaks of between four and six fragment ions per peptide and summing each of their peak areas using Skyline (University of Washington, MacCoss Lab) and normalized to a set of control peptides from highly abundant proteins found in all samples.

### Plasma levels of VVD-133214

Calibrators were prepared using commercially available mouse plasma with $K_2$-EDTA as the anticoagulant. Frozen plasma samples collected from the tumour growth study were thawed and extracted using protein precipitation with acetonitrile containing internal standard, followed by liquid chromatography–tandem mass spectrometry analysis. A Sciex 5500-QTRAP and a 6500-QTRAP linear ion trap operated in positive-mode electrospray–APCI ionization with detection by multiple-reaction monitoring were used for instrumental analysis. A Kinetex, biphenyl 2.1 × 50 $mm^2$, 2.6 µm (Phenomenex) high-performance liquid chromatography column was used with a gradient comprising water/0.1% formic acid (A) and acetonitrile/0.1% formic acid (B, varying by 5–95%), at a flow rate of 0.65 ml $min^{-1}$ and with a total run time of 2.5 min.

### Data and statistical analysis

All data were analysed using GraphPad Prism software v.9 to generate dose–response curves. All tumour volume and body mass data were analysed by two-way ANOVA with post hoc analyses (Tukey's multiple-comparison test). Pharmacodynamic biomarker assessments were analysed by one-way ANOVA. Data are presented as means ± s.e.m.

### Inclusion and ethics statement

All individuals who participated in the conceptualization, design, resourcing, execution and supervision of experiments described in this manuscript have fulfilled the criteria for authorship required by Nature Portfolio journals and have been included as authors. Their involvement was crucial in shaping and executing these studies. Individual roles and responsibilities are described in the author contribution statement. This research did not result in stigmatization, discrimination or personal risk to participants.

### Reporting summary

Further information on research design is available in the Nature Portfolio Reporting Summary linked to this article.

## Data availability

The structural data have been deposited in wwPDB under IDs 7GQS, 7GQT and 7GQU. The mass spectrometry proteomics data have been deposited to the ProteomeXchange Consortium via the PRIDE partner repository[38] with the dataset identifier PXD046214. These data can be accessed with the following username (reviewer_pxd046214@ebi.ac.uk) and password (5VPbwpt0). Proteomics analysis was performed using the *Homo sapiens* (2016) and *Mus musculus* (2017) UniProt Fasta databases. Source data are provided with this paper.


36. Schwanhäusser, B. et al. Global quantification of mammalian gene expression control. *Nature* **473**, 337–342 (2011).
37. Sommers, J. A. et al. A high-throughput screen to identify novel small molecule inhibitors of the Werner Syndrome Helicase-Nuclease (WRN). *PLoS One* **14**, e0210525 (2019).
38. Perez-Riverol, Y. et al. The PRIDE database resources in 2022: a hub for mass spectrometry-based proteomics evidences. *Nucleic Acids Res.* **50**, D543–d552 (2022).
39. Diederichs, K. & Karplus, P. A. Improved R-factors for diffraction data analysis in macromolecular crystallography. *Nat. Struct. Biol.* **4**, 269–275 (1997).
40. Karplus, P. A. & Diederichs, K. Linking crystallographic model and data quality. *Science* **336**, 1030–1033 (2012).



**Acknowledgements** We thank J. Bemis, R. Nishimura, S. Larsen and I. Stiller for programme administration; I. Mochalkin, E. Aitchison, H. Binch, D. Heer, E. Jochnowitz, A. L. Lambert, A. Rufer, R. Thoma, F. Schuler and M. Wittwer for valuable technical and scientific inputs; and B. Cravatt for helpful discussions and review of the manuscript.


**Author contributions** G.M.S., M.P.P. and T.M.K. conceptualized the project. Investigation was carried out by K.A.B., K.N.L., K.T.S., C.-C.W., M.A.H., A.N.S., X.S., T.G., S.K., J.C.G., D.C.R., B.L., M.E.R.-A., D.R.W., C.L.E., S.R., S.M.N., S.M.B., E.T., V.C., H.N.W., M.K.P., J.J.S., M.G.R., M.C., D.B. and I.C. Resources were the responsibility of P.P., C.C. and J.-M.P. K.A.B. wrote the original draft. Writing, review and editing were undertaken by J.P., P.P., J.-M.P., G.M.S., M.P.P. and T.M.K. K.A.B., S.K., J.P., A.T., J.S., L.E.B., R.T.A., D.S.W., G.M.S., M.P.P. and T.M.K. supervised the project.

**Competing interests** K.N.L., K.T.S., M.A.H., A.N.S., X.S., T.G., S.K., J.C.G., D.C.R., B.L., M.E.R.-A., D.R.W., C.L.E., S.R., S.M.N., S.M.B., J.P., V.C., H.N.W., M.K.P., J.J.S., D.S.W., G.M.S., M.P.P. and T.M.K. are current employees of Vividion Therapeutics. K.A.B., A.T., L.E.B., R.T.A., E.T., S.R. and C.-C.W. are former employees of Vividion Therapeutics. P.P., M.G.R., M.C., D.B., C.C. and J.-M.P. are current employees of F. Hoffmann-La Roche, Ltd.

**Additional information**


**Supplementary information** The online version contains supplementary material available at https://doi.org/10.1038/s41586-024-07318-y.



**Correspondence and requests for materials** should be addressed to Matthew P. Patricelli or Todd M. Kinsella.



**Peer review information** *Nature* thanks Nicholas Larsen and the other, anonymous, reviewer(s) for their contribution to the peer review of this work.

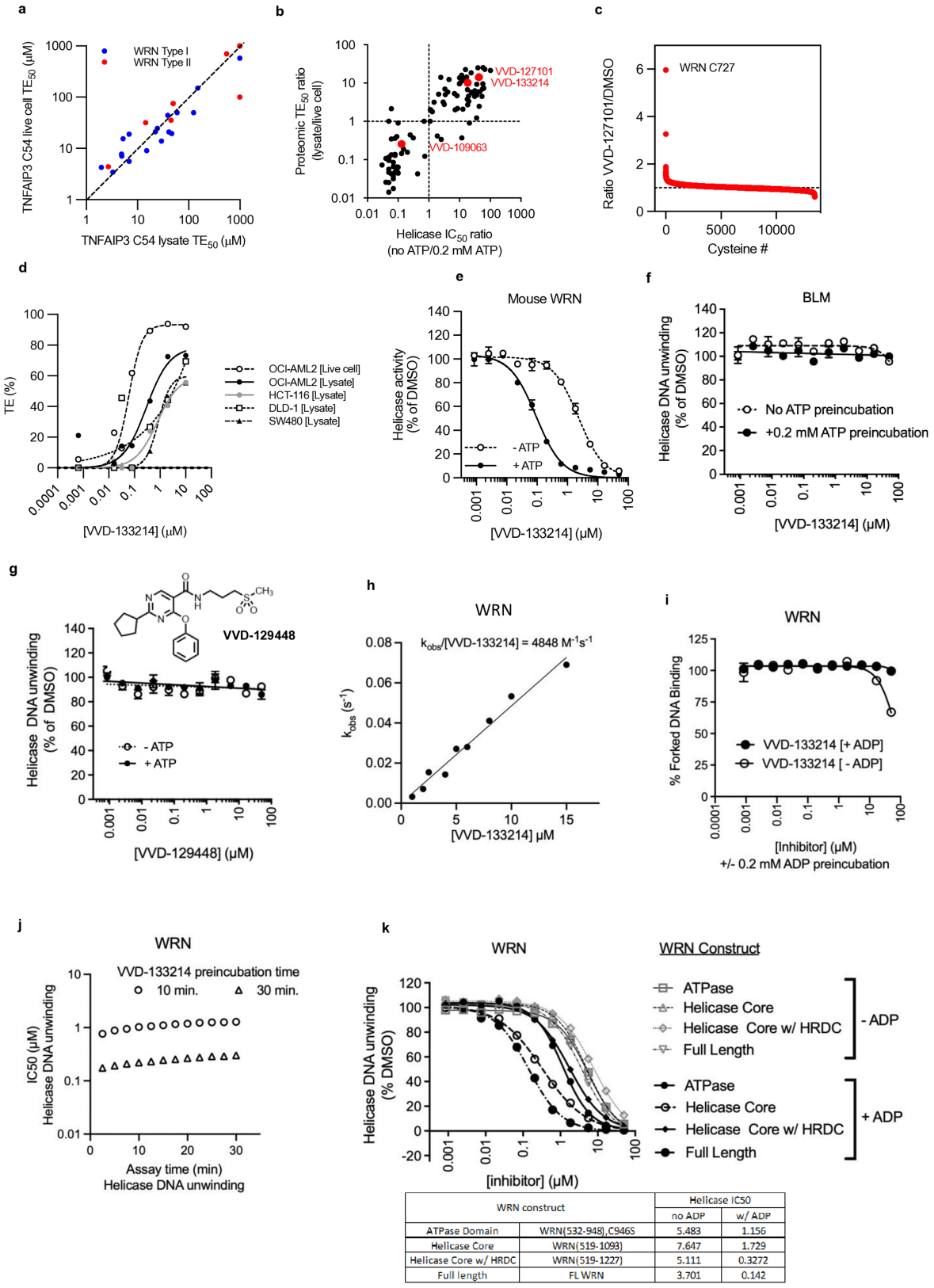


| WRN construct | | Helicase IC50 | |
|---|---|---|---|
| | | no ADP | w/ ADP |
| ATPase Domain | WRN(532-948),C946S | 5.483 | 1.156 |
| Helicase Core | WRN(519-1093) | 7.647 | 1.729 |
| Helicase Core w/ HRDC | WRN(519-1227) | 5.111 | 0.3272 |
| Full length | FL WRN | 3.701 | 0.142 |

**Extended Data Fig. 1** | See next page for caption.

**Extended Data Fig. 1 | Additional TE and helicase activity data.** (**a**) Live cell and lysate $TE_{50}$s for an off-target cysteine, TNFAIP3 C54 across all profiled compounds in WRN Type I (blue) and Type II (red) inhibitor series. (**b**) Ratios of $hWRN^{519-1227}$ helicase activity without/with 0.2 mM ATP during compound preincubation period versus ratios of $TE_{50}$s in lysates/live cells show that the ATP-cooperative compounds are the same ones that show enhanced potency in live cells. (**c**) Global TMT cysteine profiling of VVD-127101. (**d**) Dose-response curves of target engagement (WRN C727) by VVD-133214 in 4 cell lines: HCT-116 (gray circles), DLD-1 (white squares), SW480 (black triangles), and OCI-AML2 (circles). The comparison between both lysate (black circles) and live cells (white circles) is demonstrated in the screening line, OCI-AML2. (**e**) Evaluation of VVD-133214 for inhibition of mouse WRN helicase (fragment 486–1232) ($mWRN^{486-1232}$) and (**f**) hBLM activity with- and without ATP during compound preincubation period. (**g**) Lack of WRN helicase inhibition activity by a non-covalent analog of VVD-133214, VVD-129448. (**h**) Reaction kinetics for VVD-133214 were determined using intact protein mass spectrometry with recombinant WRN. The rate of covalent modification of WRN was observed over time with varying concentrations of inhibitor. Kobs/[I] was determined to be 4848 $M^{-1}s^{-1}$ (**i**) Forked DNA binding of $hWRN^{519-1227}$ in presence of VVD-133214 with- and without ADP preincubation via HTRF. (**j**) Lack of time-dependent inhibition of WRN helicase activity by VVD-133214 after helicase reaction is initiated. (**i**) Evaluation of VVD-133214 on helicase activity of several WRN constructs (ATPase domain $hWRN^{532-948, C946S}$, Helicase Core $hWRN^{519-1093}$, Helicase Core with HRDC domain $hWRN^{519-1227}$, and full length WRN $hWRN^{1-1432}$). Data are presented as means ± SEM.

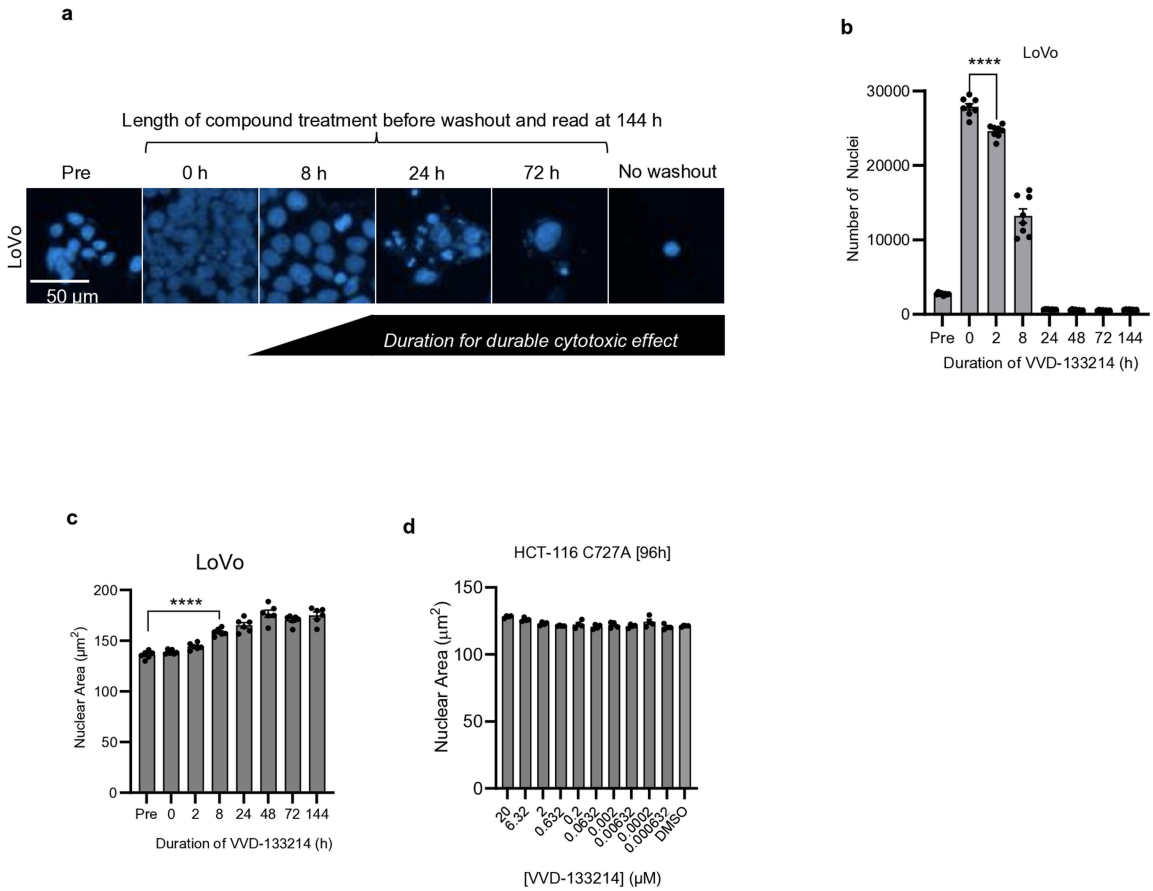


**Extended Data Fig. 2 | VVD-133214 inhibits growth in MSI-high cells.** (**a**) Short-term treatment of Lovo cells with 2 µM VVD-133214 followed by a washout of the compound for a 6-day assay assessing nuclear number (**b**) and nuclear area (**c**) (n = 7-8 biologically independent samples). (**d**) No effect on nuclear area was observed following 4-day treatment of mutant HCT-116 WRN C727A cells at any concentration tested (n = 4 biologically independent samples). Data are means +/− SEM and were analyzed by one-way ANOVA. **** p<0.0001.

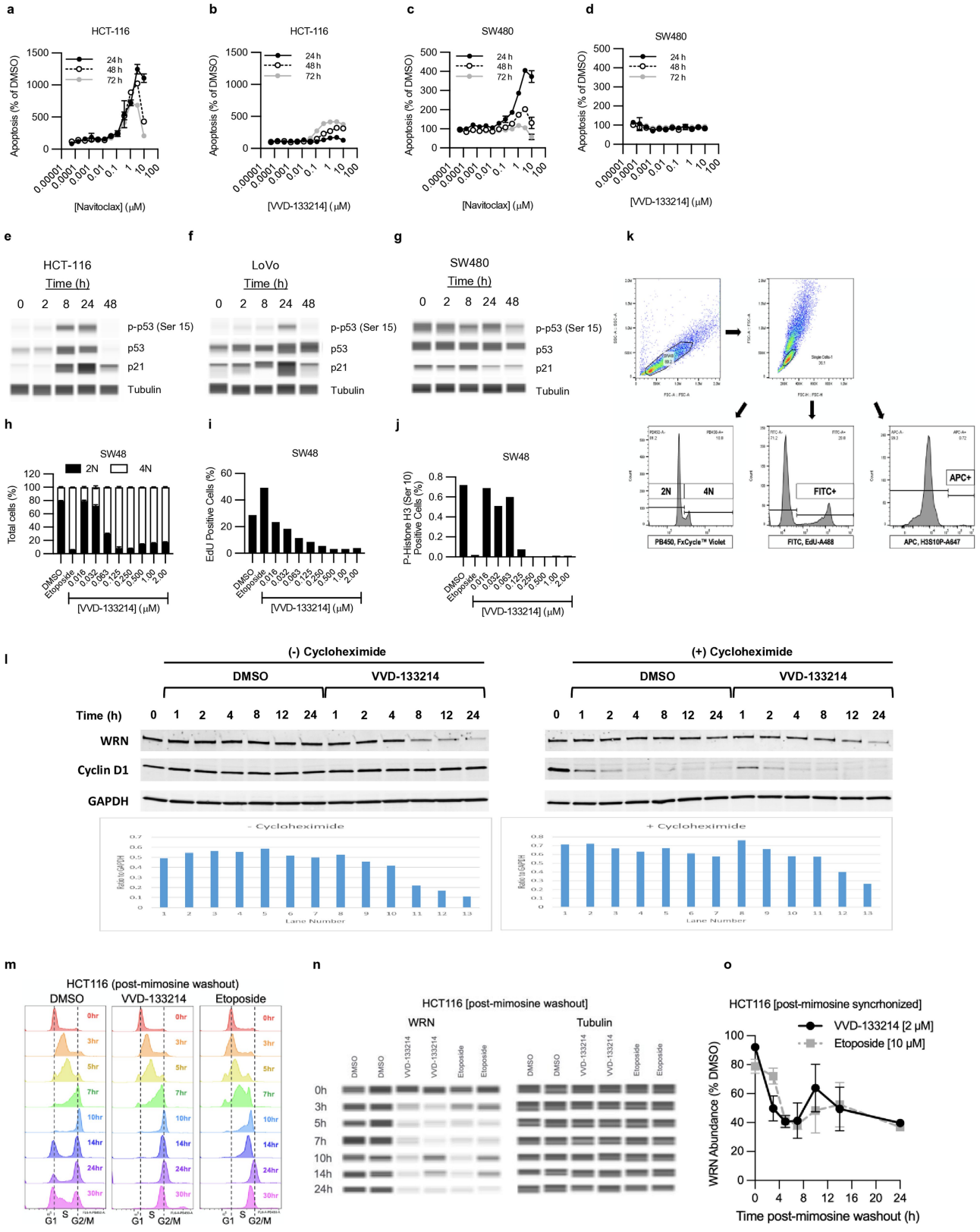


**Extended Data Fig. 3** | See next page for caption.

**Extended Data Fig. 3 | Time course of p53 pathway activation, cell cycle arrest, and apoptosis by VVD-133214.** Time course of dose-response of Navitoclax (**a**,**c**) or VVD-133214 (**b**,**d**) for apoptosis as measured by Real-time Glo Annexin V assay in MSI-high HCT-116 cells (**a**,**b**) or MSS SW480 cells (**c**,**d**). DNA damage pathway activation time course assessed by Simple Western™ following 2 μM VVD-133214 treatment in MSI-High HCT-116 (**e**), MSI-high LoVo (**f**), or MSS SW480 (**g**). Tubulin was used as a protein loading control. Columns represent individual samples. Dose-response of VVD-133214 or etoposide at 2 μM after 48 h of treatment for flow cytometry based cell cycle assessment of 2 N and 4 N DNA content in SW48 cells (**h**). (**i**) Percentage of cells in S-phase by EdU labeling. (**j**) Percentage of cells in mitosis by phospho-histone H3 (Ser10) staining. (**k**) Gating strategies for determining DNA content, EdU incorporation and phospho-Histone H3 (Ser10). (**l**) Time course of cycloheximide chase in HCT-116 cells upon treatment with 1 μM VVD214. WRN degradation occurs similarly in the presence or absence of cycloheximide suggesting that it is not translationally mediated. Cyclin D1 was utilized as a marker for cycloheximide activity (half-life of approximately 30 min). (**m**-**o**) HCT-116 cells were synchronized for 12 h with 0.5 mM mimosine, washed out, treated with 2 μM VVD-133214, 10 μM etoposide or DMSO and then analyzed over time for cell cycle progression (flow cytometry) (**m**) and WRN protein expression (Simple Western) (**n**). (**o**) Quantitation of the Simple Western data depicted in (**n**). Data are presented as means ± SEM.

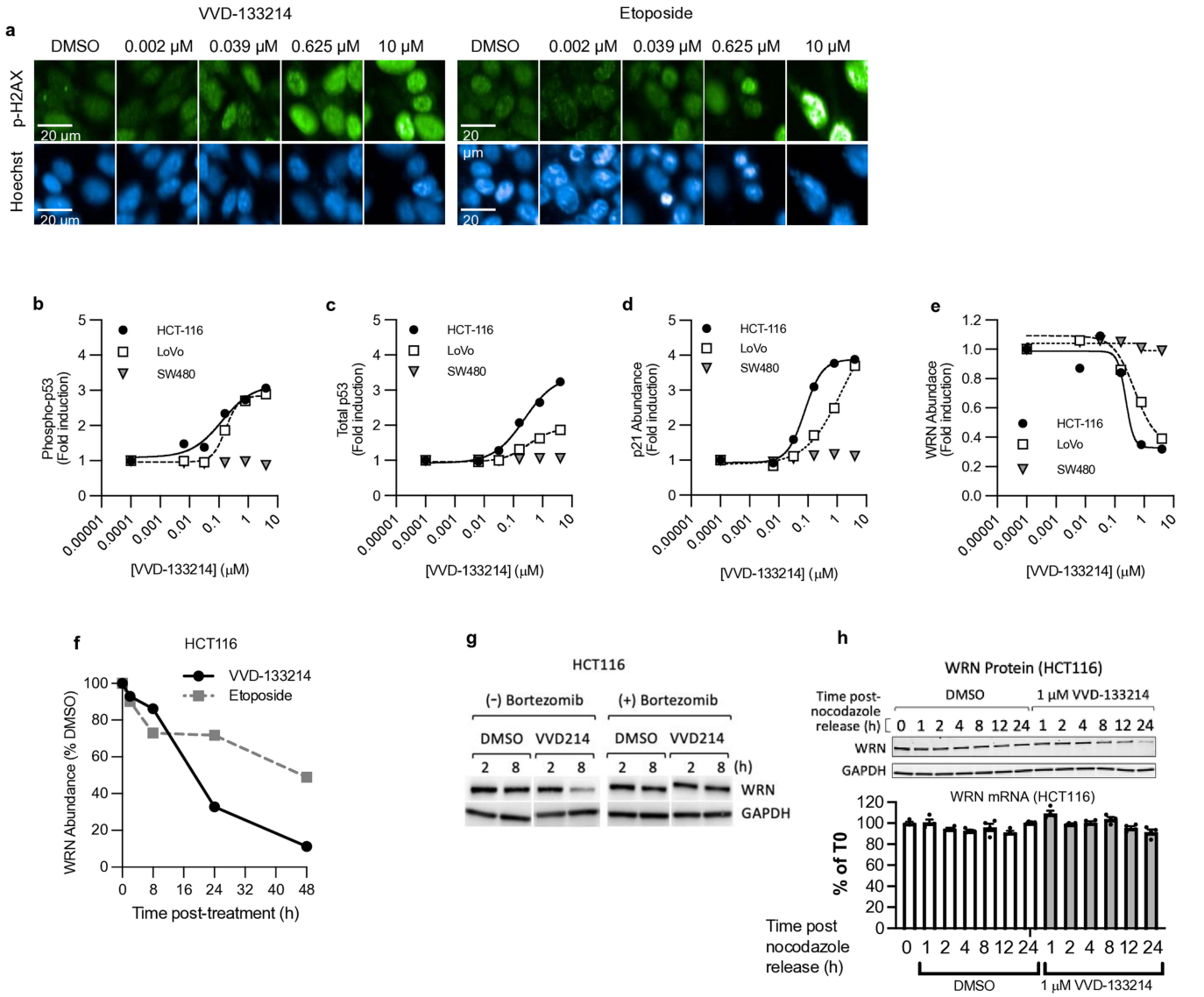


**Extended Data Fig. 4 | DNA damage and repair response in MSI-high cells.** (**a**) Representative images of phospho-H2AX (Ser139) in MSI-high RKO cells with VVD-133214 or etoposide for 96 h. (**b**-**e**) Quantitation of Simple Western data from Fig. 4d showing effects of VVD-133214 treatment on phospho-p53 (Ser15) (**b**), total p53 (**c**), p21 (**d**), and WRN (**e**) in HCT-116 (MSI), RKO (MSI), and SW480 (MSS) cells. (**f**) Time course of compound-induced loss of WRN protein in HCT-116 cells treated with VVD-133214 or Etoposide (western blot quantitation normalized to tubulin expression; n = 1). (**g**) Rescue of VVD-133214-induced loss of WRN protein in the presence of 10 μM Bortezomib. Time points beyond 8 h could not be accurately assessed due to induction of apoptosis at later time points when using Bortezomib in HCT-116 cells. (**h**) Kinetic analysis of WRN protein and mRNA levels in Nocodazole synchronized HCT-116 cells demonstrating that WRN protein and mRNA are not cell cycle regulated (n = 4, technical replicates). Micrographs are representative of two independent experiments with similar results.

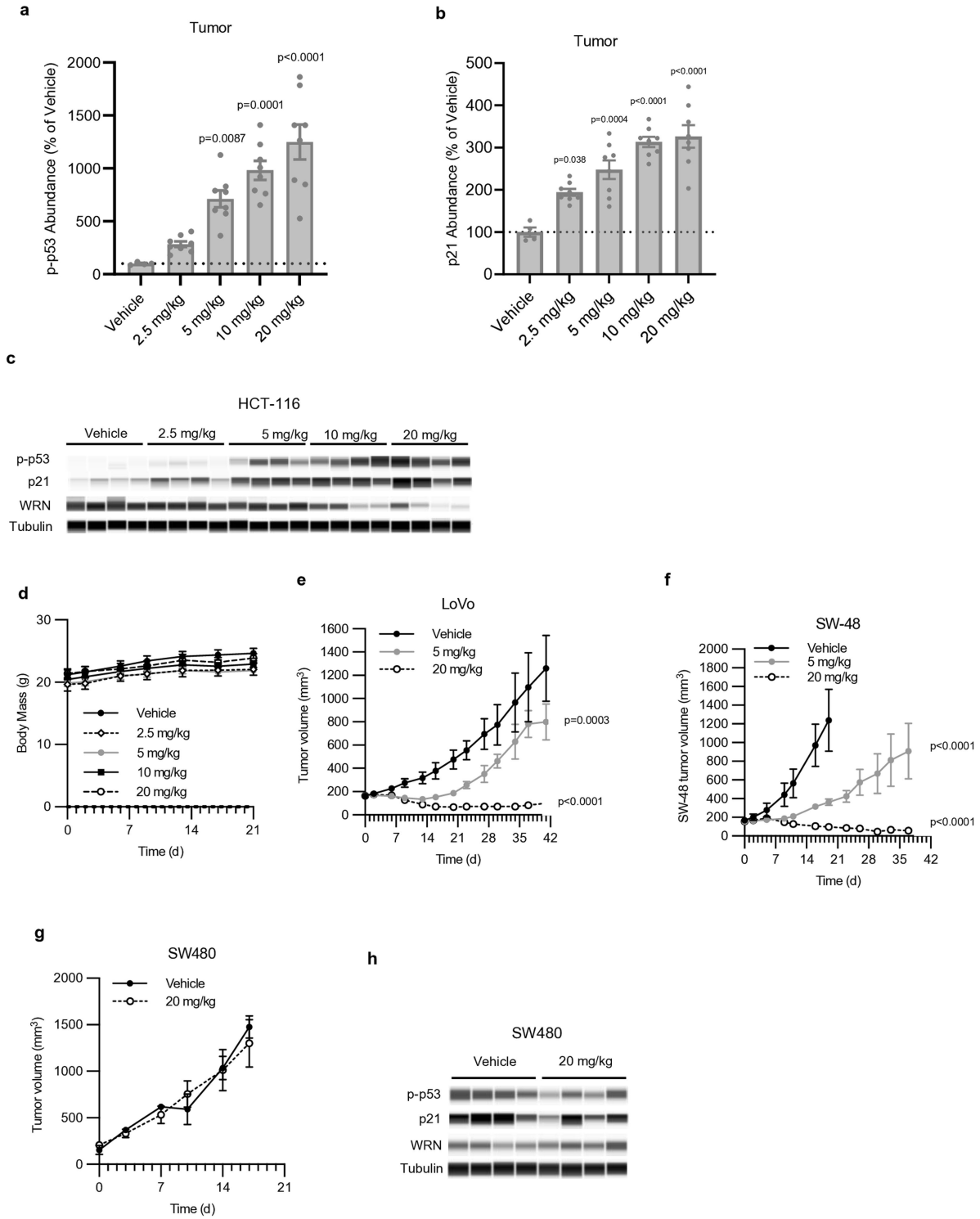


**Extended Data Fig. 5 | Tumor growth inhibition and PD in colorectal cancer xenograft models in mice.** VVD-133214 was dosed daily at 2.5, 5, 10, or 20 mg/kg via oral administration for 4 days. HCT-116 tumor tissue was collected at 2 or 24 h after the last dose (n = 4 group) and p-p53 (Ser15) (**a**) and p21 (**b**) normalized to tubulin were quantified by Simple Western. Tumor growth was assessed in female homozygous Foxn1 <nu> mice dosed orally with 2.5, 5, 10, or 20 mg/kg VVD-133214 every day for 3 weeks and p-p53 (Ser15), p21, and WRN protein levels were measured by Simple Western with tubulin as a loading control (**c**). Treatment did not impact body-mass (**d**). Additional models (n = 4–8/group) were tested for tumor growth inhibition in mice including MSI-H LoVo (**e**) and SW48 (**f**) and MSS SW480 (**g**). Markers of WRN inhibition were unchanged in MSS SW480 xenografts (**h**). Data are means +/− SEM. Data were analyzed by one-way ANOVA.

**a**

| Model | Tumor type | Treatment history | Tumor status | Site | Histology | MMR mutations | P53 mutations | TMB |
|---|---|---|---|---|---|---|---|---|
| CTG-0065 | Colorectal | Naive | Primary | Colon | Adenocarcinoma | MSH2; MSH6 | Y205C, R181C | 34.75 |
| CTG-0067 | Colorectal | Not available | Metastatic | Liver | Adenocarcinoma | MSH6; PMS2 | WT | 19.25 |
| CTG-0092 | Colorectal | Not available | Primary | Rectum | Adenocarcinoma | MLH1; MSH2; MSH6 | R273C | 27.71 |
| CTG-0117 | Colorectal | Naive | Primary | Colon | Adenocarcinoma | MSH6 | I255T | 27.33 |
| CTG-0374 | Colorectal | Not available | Primary | Colon | Adenocarcinoma | MLH1; MSH2; MSH6; PMS2 | WT | 52.00 |
| CTG-0652 | Colorectal | Not available | Primary | Colon | Adenocarcinoma | MSH6; PMS2 | WT | 30.37 |
| CTG-0978 | Colorectal | Not available | Metastatic | Liver | Not available | MLH1; PMS2 | L257R, P152L | 30.84 |

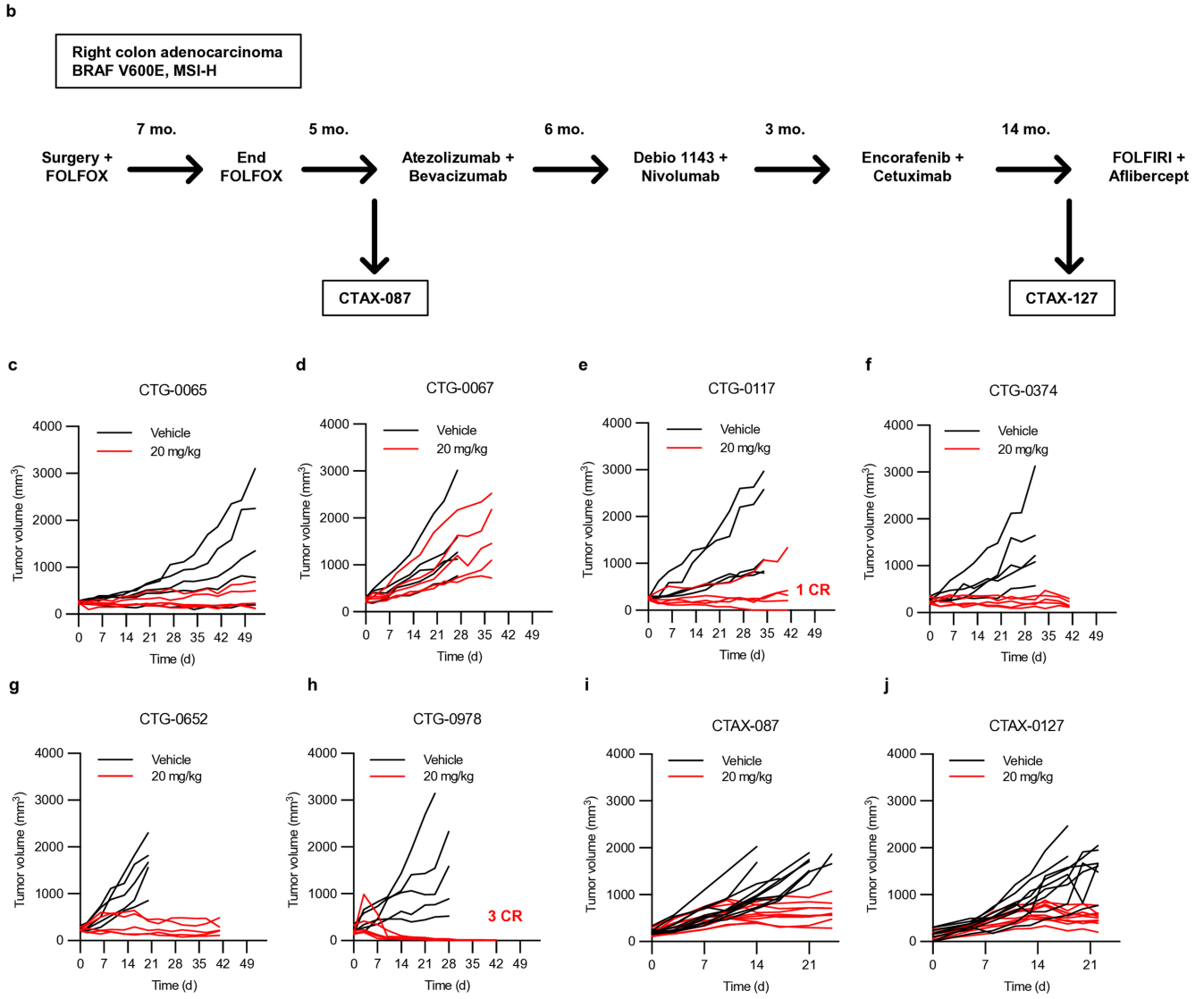


**Extended Data Fig. 6 | Characterization of PDX models.** (**a**) Description of PDX models. TMB = tumor mutational burden. (**b**) History of treatment for immunotherapy-refractory PDX model. (**c**-**j**) Spider plots of individual mice bearing the indicated PDX models treated with once-daily oral dosing of VVD-133214 at 20 mg/kg. CR = complete response.

**Extended Data Table 1 | In vitro performance measures of VVD-133214**

| Assay Type | Measure ± STD, replicate number |
|---|---|
| **$TE_{50}$ in lysate, OCI-AML2** | 0.58 ±0.44 μM, n=6 |
| **$TE_{50}$ in cell, OCI-AML2** | 0.065 ±0.033 μM, n=2 |
| **kinact/Ki (ratio, 2nd order rate constant)** | 4848 $M^{-1}$ $s^{-1}$ |
| **Kinact** | > 0.15 $s^{-1}$ |
| **Ki** | > 15 μM |
| **GSH, $k_{obs}$/[I]** | 0.0245 $M^{-1}s^{-1}$ |
| **$IC_{50}$ $hWRN^{519-1227}$ helicase DNA unwinding [+ ATP preincubation]** | 0.13 μM ±0.015 μM, n=16 |
| **$IC_{50}$ $hWRN^{519-1227}$ helicase DNA unwinding [- ATP preincubation]** | 2.3 μM ±0.39 μM, n=16 |
| **$IC_{50}$ C727A $hWRN^{519-1245}$ helicase DNA unwinding [+/- ATP preincubation]** | Not active |
| **$IC_{50}$ $hBLM^{536-1298}$ helicase DNA unwinding [+/- ATP preincubation]** | Not active |
| **$IC_{50}$ $mWRN^{486-1232}$ helicase DNA unwinding [+ ATP preincubation]** | 0.093 μM, n=2 |
| **$GI_{50}$ in HCT-116 WT (MSI-H)** | 0.066 ±0.007 μM, n=2 |
| **$GI_{50}$ in HCT-116_C727A (MSI-H)** | >20 μM, n=2 |
| **$GI_{50}$ in SW480 (MSS)** | >20 μM, n=2 |

Data are means +/− SEM.

**Extended Data Table 2 | Data collection and refinement statistics**

| | ADP (7GQS) | ATP (7GQT) | VVD-133214 + ADP (7GQU) |
|---|---|---|---|
| **Data collection** | | | |
| Space group | P 1 $2_1$ 1 | P 1 $2_1$ 1 | $P2_12_12_1$ |
| Cell dimensions | | | |
| *a*, *b*, *c* (Å) | 50.1, 90.1, 53.8 | 50.2, 90.2, 54.0 | 46.3, 83.8, 119.6 |
| α, β, γ (°) | 90, 102.5, 90 | 90, 102.8, 90 | 90, 90, 90 |
| Resolution (Å)* | 52.5-1.57 (1.69-1.57) | 52.7-2.19 (2.34-2.19) | 68.6-1.54 (1.65-1.54) |
| $R_{sym}$* | 0.076 (1.171) | 0.178 (1.187) | 0.046 (0.862) |
| $\langle I / \sigma(I) \rangle$* | 14.5 (1.5) | 6.6 (1.3) | 15.5 (1.4) |
| $CC_{1/2}$* | 0.999 (0.581) | 0.988 (0.451) | 0.999 (0.723) |
| Completeness (%)* | 92.1 (62.6) | 88.5 (50.0) | 94.8 (59.4) |
| Redundancy* | 7.0 (7.0) | 4.2 (3.8) | 6.6 (6.5) |
| **Refinement** | | | |
| Resolution (Å) | 48.9-1.57 | 52.7-2.213 | 43.1-1.54 |
| No. unique reflections | 44254 (661) | 15145 (142) | 57681 (651) |
| $R_{work}$ / $R_{free}$ | 0.1754 / 0.2185 | 0.2048 / 0.2630 | 0.1795 / 0.2088 |
| No. atoms | | | |
| Protein | 3435 | 3346 | 3392 |
| Ligand/ion | 39 | 34 | 95 |
| Water | 260 | 68 | 204 |
| *B*-factors | | | |
| Protein | 36.13 | 41.81 | 39.46 |
| Ligand/ion | 41.79 | 37.6 | 29.12 |
| Water | 37.43 | 30.54 | 39.7 |
| R.m.s. deviations | | | |
| Bond lengths (Å) | 0.012 | 0.006 | 0.009 |
| Bond angles (°) | 1.28 | 0.73 | 1.14 |

*Values in parentheses are for highest-resolution shell. *R*-values[39] and $CC_{1/2}$ (ref. 40) are defined as previously described.

nature portfolio

Corresponding author(s): Todd M. Kinsella and Matthew P Patricelli

Last updated by author(s): March 1, 2024

# Reporting Summary

Nature Portfolio wishes to improve the reproducibility of the work that we publish. This form provides structure for consistency and transparency in reporting. For further information on Nature Portfolio policies, see our Editorial Policies and the Editorial Policy Checklist.

## Statistics

For all statistical analyses, confirm that the following items are present in the figure legend, table legend, main text, or Methods section.

| n/a | Confirmed |
|---|---|
| ☐ | ☒ The exact sample size (*n*) for each experimental group/condition, given as a discrete number and unit of measurement |
| ☐ | ☒ A statement on whether measurements were taken from distinct samples or whether the same sample was measured repeatedly |
| ☐ | ☒ The statistical test(s) used AND whether they are one- or two-sided<br>*Only common tests should be described solely by name; describe more complex techniques in the Methods section.* |
| ☐ | ☒ A description of all covariates tested |
| ☐ | ☒ A description of any assumptions or corrections, such as tests of normality and adjustment for multiple comparisons |
| ☐ | ☒ A full description of the statistical parameters including central tendency (e.g. means) or other basic estimates (e.g. regression coefficient) AND variation (e.g. standard deviation) or associated estimates of uncertainty (e.g. confidence intervals) |
| ☐ | ☒ For null hypothesis testing, the test statistic (e.g. *F*, *t*, *r*) with confidence intervals, effect sizes, degrees of freedom and *P* value noted<br>*Give P values as exact values whenever suitable.* |
| ☒ | ☐ For Bayesian analysis, information on the choice of priors and Markov chain Monte Carlo settings |
| ☒ | ☐ For hierarchical and complex designs, identification of the appropriate level for tests and full reporting of outcomes |
| ☐ | ☒ Estimates of effect sizes (e.g. Cohen's *d*, Pearson's *r*), indicating how they were calculated |

*Our web collection on statistics for biologists contains articles on many of the points above.*

## Software and code

Policy information about availability of computer code

| | |
|---|---|
| Data collection | Compass V6 was used for Jess Western data collection (Bio-Techne). CytExpert V2.6 was used for flow cytometry data collection on a Beckman Coulter CytoFLEX instrument (Beckman Coulter). Xcalibur (V4.5.445.18, Thermo Scientific) was used for mass spectrometry data collection. Harmony V4.9 (Perkin Elmer) was used for Operetta CLS image aquisition. Cell-titer glow (cell proliferation) assays were measured on a BMG Labtech Clariostar instrument with software v5.7 for luminescence. |
| Data analysis | Compass V6 was used for Jess Western data analysis (Bio-Techne). FlowJo V10 (FlowJo,LLC) was used for flow cytometery data analysis. Skyline V21.2.0.369 (MacCoss Lab, Univ. Washington) was used for mass spectrometry data analysis. Harmony V4.9 (Perkin Elmer) was used for Operetta CLS image analysis (nuclear count/size). PRISM V10 (Graphpad) was used for general data analysis (dose response curve fitting, statistics, figure/graphs). Cell-titer glow luminscence data was analyzed using mars V4.0 (BMG Labtech). |

For manuscripts utilizing custom algorithms or software that are central to the research but not yet described in published literature, software must be made available to editors and reviewers. We strongly encourage code deposition in a community repository (e.g. GitHub). See the Nature Portfolio guidelines for submitting code & software for further information.

## Data

Policy information about availability of data

All manuscripts must include a data availability statement. This statement should provide the following information, where applicable:

- Accession codes, unique identifiers, or web links for publicly available datasets
- A description of any restrictions on data availability
- For clinical datasets or third party data, please ensure that the statement adheres to our policy

The structural data has been deposited into the wwPDB under IDs 7GQS, 7GQT, 7GQU and the files can be accessed under group ID G_1002280 and password (pagodan) from a group deposition account deposit@deposit.rcsb.org. The mass spectrometry proteomics data have been deposited to the ProteomeXchange Consortium via the PRIDE partner repository 43 with the dataset identifier PXD046214. This data can be accessed with the following username (reviewer_pxd046214@ebi.ac.uk) and password (5VPbwpt0). Proteomics analysis was performed using the Homo sapiens (2016) and Mus musculus (2017) UniProt Fasta database. All other data supporting the findings are contained in the manuscript and supporting data files.

## Research involving human participants, their data, or biological material

Policy information about studies with human participants or human data. See also policy information about sex, gender (identity/presentation), and sexual orientation and race, ethnicity and racism.

| | |
|---|---|
| Reporting on sex and gender | not applicable |
| Reporting on race, ethnicity, or other socially relevant groupings | not applicable |
| Population characteristics | not applicable |
| Recruitment | not applicable |
| Ethics oversight | not applicable |

Note that full information on the approval of the study protocol must also be provided in the manuscript.

# Field-specific reporting

Please select the one below that is the best fit for your research. If you are not sure, read the appropriate sections before making your selection.

☒ Life sciences ☐ Behavioural & social sciences ☐ Ecological, evolutionary & environmental sciences

For a reference copy of the document with all sections, see nature.com/documents/nr-reporting-summary-flat.pdf

# Life sciences study design

All studies must disclose on these points even when the disclosure is negative.

| | |
|---|---|
| Sample size | No statistical methods were used to pre-determine sample size. Experimental samples sizes are described in detail within the figure legends and methods section. Unless otherwise stated, experiments were performed in biological triplicate or quadruplicate. In vivo tumor growth inhibition experiments using cell-line derived xenograft models were conducted with 4-8 animals per group based on previous experience with the selected models (and the observed variability of tumor growth during model optimization). In vivo tumor growth inhibition experiments using patient-derived xenograft models were conducted with 10 animals per group and individual spider plots are depicted in figures. For all in vivo studies statistics are noted in the figures, and results were highly signficant ($p<0.01$) indicating that group sizes were sufficient for the magnitude of effects observed. |
| Data exclusions | No data exclusions were implemented |
| Replication | The exact number of experiment replications and biological replicates for experiments performed on cells or mice are noted in the figure legends. |
| Randomization | Randomization methods were utilized in all tumor xenograft studies (cell line derived and patient-derived models) such that each group had a similar mean and SEM at the start of the study. Sample randomization is not relevant to the in vitro cell and biochemical studies. |
| Blinding | Blinding was not utilized in any experiments. We have not set up the internal processes necessary for blinding in vivo studies to the people dosing animals. Tumor growth measurements are not subjective, and are taken by multiple researchers over the course of each study. |

# Reporting for specific materials, systems and methods

We require information from authors about some types of materials, experimental systems and methods used in many studies. Here, indicate whether each material, system or method listed is relevant to your study. If you are not sure if a list item applies to your research, read the appropriate section before selecting a response.

## Materials & experimental systems

| n/a | Involved in the study |
|---|---|
| ☐ | ☒ Antibodies |
| ☐ | ☒ Eukaryotic cell lines |
| ☒ | ☐ Palaeontology and archaeology |
| ☐ | ☒ Animals and other organisms |
| ☒ | ☐ Clinical data |
| ☒ | ☐ Dual use research of concern |
| ☒ | ☐ Plants |

## Methods

| n/a | Involved in the study |
|---|---|
| ☒ | ☐ ChIP-seq |
| ☐ | ☒ Flow cytometry |
| ☒ | ☐ MRI-based neuroimaging |

# Antibodies

Antibodies used

(1) Phospho-H2AX Immunofluorescence assay antibodies: anti-phospho-H2AX antibody (Catalog No. NB100-74435; Novus Biologics; Littleton, CO), goat anti-mouse secondary antibody conjugated to Alexa Fluor 488 (Catalog No. A-32723; Thermo Fisher Scientific)
(2) Antibodies utilized in Simple Western assays: anti-WRN (Catalog No. CST4666; Cell Signaling Technology; Danvers, MA), anti-p53 (Catalog No. 9282;), anti-phospho-p53 (Catalog No. 9284T), anti-alpha-tubulin (Catalog No. 2125T) or anti-p21 (Catalog No. ab109520; Abcam; Cambridge, UK). The secondary antibody was provided in the Anti-Rabbit Detection Module Chemiluminescence package (Catalog No. DM-001; Bio-Techne) or the Anti-Mouse Detection Module Chemiluminescence package (Catalog No. DM-002; Bio-Techne).
(3) Antibodies used for flow cytometry: phospho-Histone H3 (Ser10) rabbit monoclonal antibody (mAb) (Alexa Fluor 647 Conjugate; Catalog No. 3458; Cell Signaling Technology; Danvers, MA)
Antibody dilutions are noted in the methods section.

Validation

(1) anti-phospho-H2AX antibody (Catalog No. NB100-74435; Novus Biologics; Littleton, CO) is listed as validated by manufacturer using "Biological Strategies Validation"- These strategies use defined biological or chemical modulation of protein expression to demonstrate antibody specificity to the target protein. The data is compared across multiple cell lines including positive and negative expressing cells, and multiple species, if applicable. Further, this antibody was assessed by the authors of the manuscript using positive control compounds, such as Etoposide, known to induce DNA damage and subsequent DNA damage responses that include increases in phospho-H2AX.
(2) anti-WRN (Catalog No. CST4666; Cell Signaling Technology; Danvers, MA) was tested by the manufacturer in HeLa, Jurkat, and Ramos cell extracts and produced the appropriate sized band in western blot experiments. No other validation is described by the manufacturer.
(3) anti-p53 (Catalog No. 9282; Cell Signaling Technology; Danvers, MA) was tested by the manufacturer in 293, H29 and Cos cell extracts and produced the appropriate sized band in western blot experiments. No other validation is described by the manufacturer.
(4) anti-phospho-p53 (Catalog No. 9284T; Cell Signaling Technology; Danvers, MA) was tested by the manufacturer in western blot analysis using a purified recombinant p53 fusion protein phosphorylated by DNA-PK and produced the appropriate sized band in western blot experiments. No other validation is described by the manufacturer.
(5) anti-alpha-tubulin (Catalog No. 2125T; Cell Signaling Technology; Danvers, MA) was tested by the manufacturer in western blot analysis of extracts from C6, COS-7, NIH/3T3 and HeLa cells and produced the appropriate sized band in western blot experiments. No other validation is described by the manufacturer.
(6) anti-p21 (Catalog No. ab109520; Abcam; Cambridge, UK) was tested by the manufacturer in western blot analysis of extracts from MCF7, HeLa, HEK293, HUVEC, LnCaP, U87 MG or HEK-293T cell lysates. No other validation is described by the manufacturer.
(7) Phospho-Histone H3 (Ser10) (D2C8) XP® Rabbit mAb (Alexa Fluor® 647 Conjugate)(Catalog No. 3458; Cell Signaling Technology; Danvers, MA) detects endogenous levels of histone H3 only when phosphorylated at Ser10. The manufacturer states that the antibody does not cross-react with other phosphorylated histones or with acetylated histones. The manufacturer states the antibody has been tested in-house for direct flow cytometry and immunofluorescent analysis in human cells

# Eukaryotic cell lines

Policy information about cell lines and Sex and Gender in Research

Cell line source(s)

Cell lines
HCT-116 cells (ATCC, CCL-228), LoVo (CCL-229), RKO (CRL-2577), SW48 (CCL-231), DLD-1 (CCL-221), OCI-AML2 (CVCL_1619) and SW480 tumor cells (CCL-228) were cultured according to the manufacturer's instructions. WRN C727 mutant HCT-116 cells were generated by electroporation with Cas9 nuclease (Integrated DNA Technologies (IDT),1081059), CRISPR-Cas9 trans-activating CRISPR RNA (IDT, 1072532) pre-hybridized to a CRISPR RNA (crRNA) targeting the genomic region near the codon translating to C727 of the WRN gene, and a 100-bp DNA donor oligo spanning ~50 bp upstream and downstream of the C727-encoding codon. Nucleofection was completed using Lonza P3 Primary Cell 4D-Nucleofector X Kit S (Lonza V4XP-3032). The crRNA was designed using the CHOPCHOP database (https://chopchop.cbu.uib.no/). Individual cell clones were generated by limiting dilution and confirmed for C727A knock-in by Sanger sequencing. An individual mutant clone with comparable WRN expression and growth rate was selected for expansion.

Authentication

Purchased cell lines were not authenticated in house. However, cell lines purchased from the ATCC are declared as derived from authenticated stocks at ATCC, that are authenticated using STR profiling.

| | |
|---|---|
| Mycoplasma contamination | Purchased cell lines were not tested in-house for mycoplasma. However, cell lines purchased from the ATCC are declared as mycoplasma free. |
| Commonly misidentified lines (See ICLAC register) | We have checked the ICLAC register and do not believe any commonly misidentified cells lines were utilized in experiments described in this manuscript |

## Animals and other research organisms

Policy information about studies involving animals; ARRIVE guidelines recommended for reporting animal research, and Sex and Gender in Research

| | |
|---|---|
| Laboratory animals | Five-week-old female homozygous Foxn1 <nu> mice were obtained from Jackson Laboratories (Catalog No. 007850; Bar Harbor, ME). Following the acclimation period (3-7 days), each animal was inoculated subcutaneously into the right lower flank of >95% viable 10e7 tumor cells. |
| Wild animals | No wild animals were used in this study |
| Reporting on sex | All studies were conducted in female mice |
| Field-collected samples | No field collected samples were used in this study |
| Ethics oversight | Animals were maintained in accordance with the guidelines for the care and use of laboratory animals, as approved by the appropriate Institutional Animal Care and Use Committees. All animal procedures were conducted in a facility accredited by the Association for Assessment and Accreditation of Laboratory Animal Care. Studies were run at Vividion, HD Bioscience (San Diego, CA), Champions Oncology (Rockville, Maryland) (PDX models), and the Autonomous University of Barcelona. |

Note that full information on the approval of the study protocol must also be provided in the manuscript.

## Plants

| | |
|---|---|
| Seed stocks | not applicable |
| Novel plant genotypes | not applicable |
| Authentication | not applicable |

## Flow Cytometry

### Plots

Confirm that:

☒ The axis labels state the marker and fluorochrome used (e.g. CD4-FITC).

☒ The axis scales are clearly visible. Include numbers along axes only for bottom left plot of group (a 'group' is an analysis of identical markers).

☒ All plots are contour plots with outliers or pseudocolor plots.

☒ A numerical value for number of cells or percentage (with statistics) is provided.

### Methodology

| | |
|---|---|
| Sample preparation | Flow cytometry methods were as follows:<br>HCT-116, SW-48, and SW480 (2 x 10e6) cells were seeded on 10-cm plates in 10-mL medium and allowed to adhere at 37oC and 5% CO2 overnight. Cells were incubated with 2 uM VVD-133214 (24, 48, or 72 h), 2 uM etoposide (24 h), or DMSO (24 h). For compound dose response experiments, SW-48 cells were incubated with DMSO, 2 uM etoposide, or 2-fold serial dilutions of VVD-133214 at an 8-point dose response format starting at 2 uM for 48 h. Cells were incubated with 10 uM EdU (Catalog No. A10044; Invitrogen; Waltham, MA) at 37oC and 5% CO2 for 2 hours prior to harvesting.<br>Cells were harvested by trypsinization, washed, fixed in BD CytoFix Fixation Buffer (Catalog No. 554655; Fisher Scientific; Waltham, MA) for 15 minutes, and resuspended in 1 mL of 1% BSA in 1x PBS, and stored at 4oC until all samples were collected.<br>A click reaction cocktail was prepared according to calculations from the Click-iT Plus Alexa Fluor 488 Picolyl Azide Toolkit (Catalog No. C10461; Invitrogen). Samples were incubated in the reaction cocktail at 25oC away from light for 30 minutes and then pelleted at 3000 rpm for 1 minute. The supernatants were discarded, and samples were washed twice in 1% BSA and 0.1% Triton X-100 in 1x PBS. After washing, samples were resuspended in 100 mL of 1% BSA and 0.1% Triton X-100 in 1x |

PBS supplemented with phospho-Histone H3 (Ser10) rabbit monoclonal antibody (mAb) (Alexa Fluor 647 Conjugate; Catalog No. 3458; Cell Signaling Technology; Danvers, MA) at a dilution of 1:100.
Samples were incubated at 25°C away from light for 45 minutes and then pelleted at 3000 rpm for 1 minute. After discarding supernatants, cells were washed twice in 1% BSA and 0.1% Triton X-100 in 1x PBS and resuspended in 100 mL of 1% BSA and 0.1% Triton X-100 in 1x PBS supplemented with FxCycle Violet stain (Catalog No. F10347; Invitrogen) at a dilution of 1:1000. Samples were incubated at 25°C away from light for 30 minutes and then analyzed on a Beckman Coulter Cytoflex S flow cytometer using the following laser gain settings:forward scatter (FSC): 10, side scatter (SSC): 10, Pacific Blue™ Dye, V450 (PB450): 10, fluorescein isothiocyanate (FITC): 20, allophycocyanin (APC): 300. All flow cytometry data were analyzed by FlowJo software (V10.8.1; FlowJo; Ashland, OR). Experiments quantitating DNA content run with two technical replicates. Graphs depicting EdU labeling and phospho-histone H3 (Ser 10) staining depict a single sample per time point.

Instrument

Flow analysis conducted on a Beckman Coulter Cytoflex S flow cytometer using the following laser gain settings:forward scatter (FSC): 10, side scatter (SSC): 10, Pacific Blue™ Dye, V450 (PB450): 10, fluorescein isothiocyanate (FITC): 20, allophycocyanin (APC): 300.

Software

All flow cytometry data were analyzed by FlowJo software (V10.8.1; FlowJo; Ashland, OR).

Cell population abundance

20,000 cells were analyzed per sample per experiment

Gating strategy

For cell cycle analysis, debris and dead cells were excluded based on forward scatter-area (FSC-A) and side scatter-area (SSC-A) profiles. Subsequently, single cells were identified based on FSC-A and forward scatter-height (FSC-H) profiles. Single cells were then analyzed for FxCycle Violet stain (PB450), EdU-Alexa Fluor 488 (EdU-A488, FITC) and phospho-Histone H3 (Ser10) Alexa Fluor 647 (H3S10P-A647, APC) staining intensities. FxCycle Violet stain was biphasic; the population exhibiting lower intensity with the PB450 filter were deemed as having “2N” DNA content, while the population exhibiting higher intensity with the PB450 filter were deemed as “4N” DNA content. FITC-positive cells (cells exhibiting higher staining intensity than unstained cells) were classified as “EdU Positive Cells”. APC-positive cells (cells exhibiting higher staining intensity than unstained cells) were classified as “P-Histone H

☒ Tick this box to confirm that a figure exemplifying the gating strategy is provided in the Supplementary Information.